Insertion of $H_2C{=}CHX$ (X = F, Cl, Br, O^{i}Pr) into (^{t}Bu$_3$SiO)$_3$TaH$_2$ and β-X-Elimination from (^{t}Bu$_3$SiO)$_3$HTaCH$_2$CH$_2$X (X = OR): Relevance to Ziegler−Natta Copolymerizations

Stephanie A. Strazisar and Peter T. Wolczanski*

Contribution from the Baker Laboratory, Department of Chemistry and Chemical Biology, Cornell University, Ithaca, New York 14853

Received September 8, 2000

Abstract: The insertion of $H_2C{=}CHX$ (X = OR; R = Me, Et, ^{n}Pr, ^{i}Pr, $CH{=}CH_2$, Ph) into (^{t}Bu$_3$SiO)$_3$TaH$_2$ (**1**) afforded (^{t}Bu$_3$SiO)$_3$HTaCH$_2$CH$_2$X (**2**-CH$_2$CH$_2$X), which β-X-eliminated to give ethylene and (^{t}Bu$_3$SiO)$_3$-HTaX (**3**-X). β-X-elimination rates were inversely proportional to the size of R. An X-ray crystallographic study of (^{t}Bu$_3$SiO)$_3$HTaCH$_2$CH$_2$O^{t}Bu (**2**-CH$_2$CH$_2$O^{t}Bu) revealed a distorted trigonal bipyramidal structure with an equatorial plane containing the hydride and a −CH$_2$CH$_2$O^{t}Bu ligand with a staggered disposition. *erythro*- and *threo*-(^{t}Bu$_3$SiO)$_3$HTaCHDCHDOEt (**2**-CHDCHDOEt) are staggered in solution, according to ^{1}H NMR spectroscopic studies, and eliminated *cis*- and *trans*-HDC=CHD, respectively, helping verify the four-centered transition state for β-OEt-elimination. When X = F, Cl, or Br, **2**-CH$_2$CH$_2$X was not observed en route to **3**-X, signifying that olefin insertion was rate-determining. Insertion rates suggested that substantial positive charge on the substituted carbon was incurred. The reactivity of other $H_2C{=}CHX$ with **1**, and a discussion of the observations and their ramifications on the incorporation of functionalized monomers in Ziegler−Natta copolymerizations, are presented.

Introduction

The inclusion of functionality into hydrocarbon-based polyolefins can dramatically alter their microstructure and properties.[1,2] Many commercially important polymers and resins could be supplanted, provided the incorporation of functionality can be controlled and the material is inexpensive. Current post-polymer modification technology and free-radical-based copolymerizations do not meet these criteria and fail to deliver the diversity of products needed to generate interest in expanding this research direction.[2−4]

Single-site Ziegler−Natta (ZN) catalysts can polymerize ethylene at relatively low temperatures (<100 °C) and pressures (<4 atm) and can be used to generate random copolymers when an α-olefin is an additional substrate.[5−11] While the current generation of ZN catalysts can be tuned to afford hydrocarbon-based polymers with varying properties, they will tolerate only a limited number of functionalities present on the comonomer. Polar comonomers must be protected by steric bulk[12,13] and methylene spacers[14−16] and through complexation to Lewis acids[17,18] when early transition metal ZN catalysts are used. A few late transition metal catalysts will copolymerize standard conjugated polar vinyl substrates,[19−21] but less control over the polymer microstructure and the resulting properties hampers commercial applications.

Scheme 1 illustrates the generally accepted Cosseé mechanism of insertion and β-H-elimination in the polymerization of ethylene and related monomers.[22,23] As path A shows, the insertion process—in this case shown for ethylene—can be assigned a simple rate constant (k_e) for the overall event, or can be separated into microscopic olefin binding ($k_{e1}/k_{e(-1)}$) and insertion (k_{e2}) steps. Propagation rates (R_p) are ascribed to the insertion of olefin and are often first order in monomer and

(1) Boffa, L. S.; Novak, B. M. *Chem. Rev.* **2000**, *100*, 1479−1493.
(2) Padwa, A. R. *Prog. Polym. Sci.* **1989**, *14*, 811−833.
(3) Doak, K. W. In *Encyclopedia of Polymer Science and Engineering*; Mark, H. F., Ed.; John Wiley and Sons: New York, 1986; Vol. 6, pp 386-429.
(4) Hagman, J. F.; Crary, J. W. In *Encyclopedia of Polymer Science and Engineering*; Mark, H. F., Ed.; John Wiley and Sons: New York, 1985; Vol. 6, p 325.
(5) Coates, G. W. *Chem. Rev.* **2000**, *100*, 1223−1252.
(6) Brintzinger, H. H.; Fischer, D.; Mülhaupt, R.; Rieger, B.; Waymouth, R. M. *Angew. Chem., Int. Ed. Engl.* **1995**, *34*, 1143−1170.
(7) Alt, H. G.; Köppl, A. *Chem. Rev.* **2000**, *100*, 1205−1222.
(8) (a) Hlatky, G. G. *Chem. Rev.* **2000**, *100*, 1347−1376. (b) Hlatky, G. G. *Coord. Chem. Rev.* **1999**, *181*, 243−296.
(9) Resconi, L.; Cavallo, L.; Fait, A.; Piemontesi, F. *Chem. Rev.* **2000**, *100*, 1253−1346.
(10) Kaminsky, W.; Arndt, M. *Adv. Polym. Sci.* **1997**, *127*, 143−187.
(11) Bochmann, M. *J. Chem. Soc., Dalton Trans.* **1996**, 255−270.
(12) Kesti, M. R.; Coates, G. W.; Waymouth, R. M. *J. Am. Chem. Soc.* **1992**, *114*, 9679−9680.
(13) Wilén, C.-E.; Luttikhedde, H.; Hjertberg, T.; Näsmen, J. N. *Macromolecules* **1996**, *29*, 8569−8575.
(14) Klabunde, U.; Ittel, S. D. *J. Mol. Catal.* **1987**, *41*, 123−134.
(15) (a) Aaltonen, P.; Fink, G.; Löfgren, B.; Seppälä, J. *Macromolecules* **1996**, *29*, 5255−5260. (b) Aaltonen, P.; Löfgren, B. *Macromolecules* **1995**, *28*, 5353−5357.
(16) Schneider, M. J.; Schäfer, R.; Mülhaupt, R. *Polymer* **1997**, *38*, 2455−2459.
(17) Marques, M. M.; Correia, S. G.; Ascenso, T. R.; Ribeiro, A. F. G.; Gomes, P. T.; Dias, A. R.; Foster, P.; Rausch, M. D.; Chien, J. C. W. *J. Polym. Sci., Part A: Polym. Chem.* **1999**, *37*, 2457−2469.
(18) Novak, B. M.; Hiromitsu, T. *Polym. Mater. Sci. Eng.* **1999**, *80*, 45.
(19) Johnson, L. K.; Mecking, S.; Brookhart, M. *J. Am. Chem. Soc.* **1996**, *118*, 267−268.
(20) Mecking, S.; Johnson, L. K.; Wang, L.; Brookhart, M. *J. Am. Chem. Soc.* **1998**, *120*, 888−899.
(21) Ittel, S. D.; Johnson, L. K.; Brookhart, M. *Chem. Rev.* **2000**, *100*, 1169−1203.
(22) Cosseé, J. *J. Catal.* **1964**, *3*, 80−88.
(23) Collman, J. P.; Hegedus, L. S.; Norton, J. R.; Finke, R. G. *Principles and Applications of Organotransition Metal Chemistry*; University Science Books: Mill Valley, CA, 1987.

10.1021/ja003315n CCC: $20.00
Published on Web 04/25/2001

Scheme 1

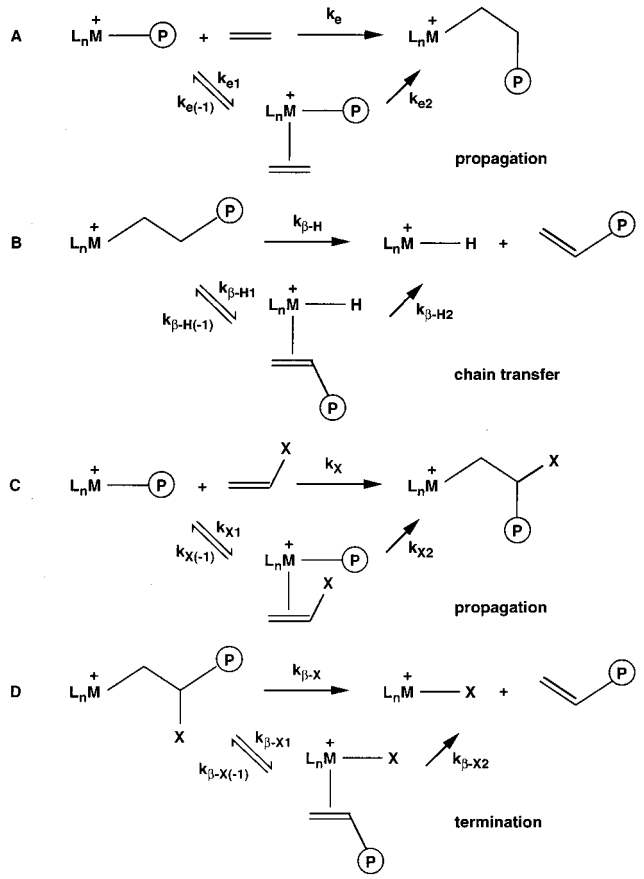

second order overall. The olefin complex is taken as a fleeting intermediate,[24] and the steady-state approximation can be applied to obtain $R_p^e = k_e[L_nMP^+][CH_2CH_2]$ and $k_e = k_{e1}k_{e2}/(k_{e(-1)} + k_{e2})$. In most cases and under most conditions, olefin coordination is considered to be fast and reversible, and the insertion step is considered rate-determining (i.e., $k_e \approx k_{e1}k_{e2}/(k_{e(-1)})$. In some late metal systems, the catalyst resting state is considered to be the alkyl-olefin complex, resulting in chain growth rates that are zero order in monomer.[25] Several studies have uncovered polymerization systems that show [monomer]^n ($n > 1$), where the propagation approaches second order in monomer. Ystenes proposed a "trigger mechanism" where coordination of two monomers is crucial,[26,27] while Resconi et al. explained similar results by invoking two rapidly interconverting forms of a catalyst resting state, with one reacting much faster than the other.[9,28,29] For the purposes of discussion herein, the straightforward mechanisms in Scheme 1 will suffice.

A similar propagation sequence describes the insertion of CH_2═CHX (path C), and in a copolymerization process, an even distribution of comonomers results if $k_e[L_nMP^+][CH_2$═$CH_2] \approx k_X[L_nMP^+][CH_2$═$CHX]$. Comonomer concentrations can be controlled to a certain extent (neat monomer being an obvious limit for liquid substrates), but each substrate also has an inherent reactivity with L_nMP^+ (k_e vs k_X). In a chain-transfer event, β-H-elimination from a growing polymer chain produces a metal hydride that is still an active polymerization catalyst (path B), but β-X-elimination from a functionalized polymer generates a species that is incapable of initiating further polymerization (path D)[30] unless it is reactivated. Chain transfer by β-H-elimination can also occur from the functionalized polymer chain, but if $k_{\beta-X}[L_nMP^+]$ is swifter than or similar to $k_e[L_nMP^+][CH_2$═$CH_2]$, only oligomers can be formed.

Scheme 2

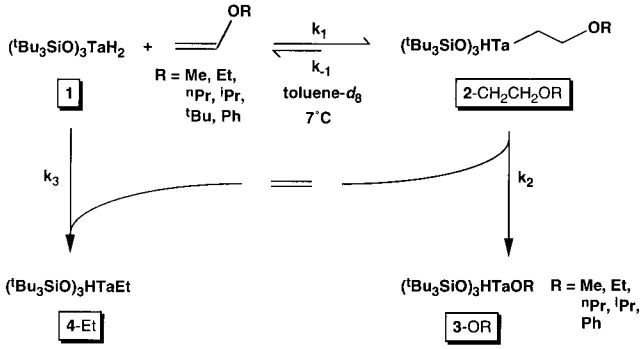

The reactivity of $(^tBu_3SiO)_3TaH_2$ (**1**)[31] with simple polar vinyl monomers (CH_2═CHX, X = OR, halide) has been examined. Dihydride **1** is less electrophilic than a typical cationic ZN catalyst, allowing relative rates of insertion and β-X-elimination to be observed as a function of X. As a consequence, inferences to propagation and termination events in true ZN systems can be made.

Results and Discussion

Vinyl Ethers. 1. Insertion and β-OR-Elimination Products. $(^tBu_3SiO)_3TaH_2$ (**1**)[31] was treated with a series of vinyl ethers (CH_2═$CHOR$, R = Me, Et, ^{n}Pr, ^{i}Pr, ^{t}Bu, Ph) in toluene-d_8 at 7 ± 1 °C, as indicated in Scheme 2. 1,2-Insertion to afford the ethyl β-ether complexes, $(^tBu_3SiO)_3HTaCH_2CH_2OR$ (**2**-CH_2CH_2OR), was observed, and none of the alternative 2,1-insertion products were evident by ^{1}H NMR spectroscopy. With the exception of **2**-$CH_2CH_2O^tBu$, the remaining **2**-CH_2CH_2OR complexes underwent an apparent β-OR-elimination to provide $(^tBu_3SiO)_3HTaOR$ (**3**-OR). Free ethylene was observed, and some formation of the known ethyl hydride derivative, $(^tBu_3SiO)_3HTaEt$ (**4**-Et),[31] was noted. All species in Scheme 2 were observed by ^{1}H NMR spectroscopy, and Table 1 lists these data, along with $^{13}C\{^1H\}$ NMR spectra that were obtained for selected compounds.

2. Verification of β-OR-Elimination. To verify that all $(^tBu_3SiO)_3HTaOR$ (**3**-OR) complexes were generated according to the insertion/β-OR-elimination pathway illustrated, some mechanistic probes were utilized. Scheme 3 indicates an alternative mechanism predicated on the direct exchange of OR for a hydride of $(^tBu_3SiO)_3TaH_2$ (**1**), which would render the stereochemistry of the byproduct olefin unchanged from the vinyl ether. Treatment of **1** with a mixture of *cis*- and *trans*-β-methoxystyrene resulted in no reaction (eq 1). Since the

$$(^tBu_3SiO)_3TaH_2 \; (\mathbf{1}) + MeOCH{=}CHPh \rightarrow \text{no reaction} \quad (1)$$

phenyl group is spatially removed from the carbon bearing the

(24) Grubbs, R. H.; Coates, G. W. *Acc. Chem. Res.* **1996**, *29*, 85−93.
(25) Johnson, L. K.; Killian, C.-M.; Brookhart, M. *J. Am. Chem. Soc.* **1995**, *117*, 6414−6415.
(26) Ystenes, M. *J. Catal.* **1991**, *129*, 383−401.
(27) Chien, J. C. W.; Yu, Z.; Marques, M. M.; Flores, J. C.; Rauch, M. D. *Polym. Sci., Part A: Polym. Chem* **1998**, *36*, 319−328.
(28) Fait, A.; Resconi, L.; Guerra, G.; Corradini, P. *Macromolecules* **1999**, *32*, 2104−2109.
(29) Resconi, L.; Fait, A.; Piemontesi, F.; Colonnesi, M.; Rychlicki, H.; Ziegler, R. *Macromolecules* **1995**, *28*, 6667−6676.
(30) For a recent example of how β-Cl-elimination interferes with the Ziegler−Natta polymerization of ethylene and vinyl chloride, see: Stockland, R. A., Jr.; Jordan, R. F. *J. Am. Chem. Soc.* **2000**, *122*, 6315−6316.
(31) Miller, R. L.; Toreki, R.; LaPointe, R. E.; Wolczanski, P. T.; Van Duyne, G. D.; Roe, D. C. *J. Am. Chem. Soc.* **1993**, *115*, 5570−5588.

Table 1. ^{1}H and ^{13}C{^{1}H} NMR Spectral Data for (^{t}Bu$_3$SiO)$_3$HTaCH$_2$CH$_2$(X/OR) (**2**-CH$_2$CH$_2$(X/OR)), (^{t}Bu$_3$SiO)$_3$HTa(X/OR) (**3**-(X/OR)), (^{t}Bu$_3$SiO)$_3$HTaR (**4**-R), and Related Complexes in C_7D_8[a–c] unless Otherwise Noted

	^{1}H NMR (δ,[a] assignment, multiplicity, J (Hz))			^{13}C{^{1}H} NMR (δ,[b] assignment)		
compound	((H$_3$C)$_3$C)$_3$	TaH[d]	other	C(*C*H$_3$)$_3$	*C*(CH$_3$)$_3$	other
(^{t}Bu$_3$SiO)$_3$TaH$_2$ (**1**)[e]	1.23	21.91		29.86	24.14	
(^{t}Bu$_3$SiO)$_3$TaHD (**1**-*d*)[e]	1.23	21.97				
2-CH$_2$CH$_2$OMe	1.27	22.35 (br)	2.04 (CH$_2$, dt, 7.8, 3.0), 3.20 (CH$_3$, s), 4.28 (CH$_2$O, t, 7.6)			
2-CH$_2$CH$_2$OCH$_2$CH$_3$[f]	1.24	22.38 (t, 3.2)	1.14 (CH$_3$, t, 6.9) 3.44 (OCH$_2$, q, 7.0), 4.25 (CH$_2$O, t, 7.6)			
2-CH$_2$CH$_2$OCH$_2$CH$_2$CH$_3$	1.25	22.38 (br)	0.89 (CH$_3$, t, 6.0) 1.57 (CH$_2$, m, 6.7) 2.14 (TaCH$_2$, dt, 3.1, 7.0), 3.39 (OCH$_2$, t, 6.6) 4.26 (CH$_2$O, t, 8.6)			
2-CH$_2$CH$_2$OPh	1.25	22.45 (br)	2.25 (CH$_2$, m) 4.82 (CH$_2$O, m) 6.6−6.7 (Ph, m)			
2-CH$_2$CH$_2$OCHMe$_2$	1.25	22.38 (t, 3.2)	1.13 (Me$_2$, d, 6.1) 2.14 (CH$_2$, m, 3.4) 3.60 (CH, sept, 6.0) 4.20 (CH$_2$O, m, 8.4)	30.65	23.66	22.77 (Me$_2$) 70.32 70.84 75.97 (OCH)
2-CH$_2$CH$_2$OCMe$_3$	1.25	22.37 (br)	1.22 (Me$_3$, s) 2.06 (CH$_2$, m)[f] 4.11 (CH$_2$O, m, 8.2)	30.80	23.78	30.60 (Me$_3$) 64.21 72.53 76.88 (CMe$_3$)
2-CH$_2$CH$_2$OCH=CH$_2$[f]	1.25	22.41	4.21 (CH$_2$O, m, 6.1) 4.30 (=CH*H*, m, 11.9, 3.1) 6.57 (OCH=, dd, 10.8, 6.3)			
3-OMe	1.28	22.86	4.15 (s)			
3-OCH$_2$CH$_3$	1.25	21.60	1.17 (CH$_3$, t, 7.0) 4.48 (CH$_2$, q, 7.0)			
3-OCH$_2$CH$_2$CH$_3$	1.27	21.16	0.86 (CH$_3$, t, 6.4) 1.59 (CH$_2$, sext, 7.0) 4.46 (CH$_2$O, t, 6.7)			
3-OCHMe$_2$	1.28	21.19	1.14 (Me$_2$, d, 6.1) 5.05 (CH, sept, 6.1)	30.78	23.71	26.47 (Me$_2$) 76.92 (OC)
3-OPh	1.25	21.60	7.1−7.2 (Ph, m)			
3-OCH=CH$_2$	1.27	21.18	4.06 (=C*H*H, d, 6.0) 4.49 (=CH*H*, d, 13.5) 5.77 (OCH=, dd, 10.8, 6.3)			
3-OCHEtCH=CH$_2$	1.28	21.26	0.82 (CH$_3$, t, 7.3) 1.92 (CH$_2$, sept, 4.0) 5.13 (CH=CH$_2$, m) 5.70 (CH, quin, 8.9)	30.78	23.65	9.37 (CH$_3$) 31.43 (CH$_2$) 87.46 (OC) 116.27 (=CH$_2$) 140.89 (=CH−)
3-OCH$_2$CH=CH$_2$	1.26	21.51	4.98 (OCH$_2$, dq, 5.5, 1.2) 5.10 (=C*H*H, dq, 10.4, 1.2) 5.20 (=CH*H*, dq, 17.1, 1.6) 5.92 (=CH−, m)			
3-OCHMe$_2$	1.28	21.19	1.14 (Me$_2$, d, 6.1) 5.05 (CH, sept, 6.1)	30.78	23.71	26.47 (Me$_2$) 76.92 (CH)
3-F	1.24	21.96 (d, 95)		30.51	23.75	
3-Cl[e]	1.23	20.03				
3-Br	1.27	19.08		30.84	24.52	
4-CH$_2$CH$_3$[e,g]	1.25	22.24 (t, 3.1)	2.15 (CH$_3$, t, 7.8) 1.76 (CH$_2$, dq, 3.4, 7.8)	30.76	23.69	16.44 (CH$_3$) 70.90 (CH$_2$)
4-CH$_2$CH$_2$CH$_3$	1.26	22.30 (t, 3.2)	0.96 (CH$_3$, t, 7.2) 1.80 (CH$_2$, dt, 3.4, 7.8) 2.33 (CH$_2$, m)			
(^{t}Bu$_3$SiO)$_3$TaOCHEtCH$_2$CH$_2$[f] (**5**-Et)	1.29		0.91 (CH$_3$, t, 7.5) 1.70 (CH$_2$, m, 6.7) 2.66 (CH*H*, m, 14.4, 5.5) 3.48 (TaCH$_2$, quin, 4.9) 4.58 (OCH, m)	31.04	23.90	11.77 (CH$_3$) 30.50 (CH$_2$Me) 42.96 (CH$_2$) 68.90 (TaCH$_2$) 89.14 (OC)
(^{t}Bu$_3$SiO)$_3$TaOCH$_2$CH$_2$CH$_2$ (**5**-H)	1.28		2.12 (TaCH$_2$, t, 7) 2.92 (CH$_2$, quin, 6.7) 4.62 (OCH$_2$, t, 6.2)			
(^{t}Bu$_3$SiO)$_3$Ta(OCH$_2$CH$_3$)$_2$ (**6**-(OEt)$_2$)	1.28		1.25 (CH$_3$, t, 7.6) 4.68 (CH$_2$, q, 7.1)			
(^{t}Bu$_3$SiO)$_3$Ta(OCH$_2$CH$_2$CH$_3$)$_2$ (**6**-(O^{n}Pr)$_2$)	1.30		1.27 (CH$_3$, t, 6) 1.78 (CH$_2$, sext, 7.6) 4.58 (CH$_2$, m, 8.3)			

[a] Referenced to the residual methyl resonance of C_7D_7H at δ 2.09. [b] Referenced to methyl of toluene-d_8 at δ 20.4 unless otherwise noted. [c] When multiplets were observed, phenomenological couplings are given. [d] Singlet unless otherwise noted. [e] See ref 31. [f] Some resonances obscured or partially obscured by solvent or ^{t}BuSiO. [g] ^{13}C {^{1}H} NMR spectrum taken in benzene-d_6 and referenced to C_6D_6 at δ 128.00.

Scheme 3

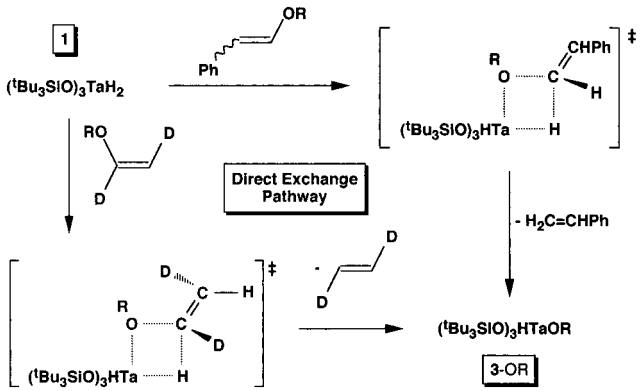

OMe substituent, a direct exchange should be relatively sterically unencumbered. An insertion/β-OR-elimination pathway requires the Ph group to occupy a sterically unfavorable α-position in the incipient ($^tBu_3SiO)_3HTaCHPhCH_2OMe$ species, and it is plausible that this interaction obviates any reaction involving a 1,2-insertion. The opposite 2,1-insertion does not occur either and may also be a consequence of the large methoxy (relative to H) substituent on the α-carbon in the putative alkyl hydride product. When excess 2-methoxypropene was added to **1**, ($^tBu_3SiO)_3HTaOMe$ (**3**-OMe) did form (eq 2), but the

$$(^tBu_3SiO)_3TaH_2 + H_2C{=}CMe(OMe) \xrightarrow[23\ ^\circ C]{C_7D_8} \underset{\mathbf{1}}{} (^tBu_3SiO)_3HTaOMe\ (\mathbf{3}\text{-OMe}) + H_2C{=}CHMe + (^tBu_3SiO)_3HTa^nPr\ (\mathbf{4}\text{-}^n\text{Pr}) \quad (2)$$

intermediate β-OMe-propyl hydride was not noted. The half-life for the appearance of **3**-OMe was significantly longer ($t_{1/2} \approx 12$ h, 23 °C) than that for the corresponding methyl vinyl ether reaction ($t_{1/2} \approx 0.75$ h, 7 °C). The propyl hydride, ($^tBu_3SiO)_3HTa^nPr$ (**4**-^{n}Pr), was also generated due to release of propene upon β-OMe-elimination, and this reaction was independently verified by the reaction of **1** and H_2C=CHMe. From these observations, steric factors appear more critical at the α-carbon, but β-carbon substituents can also significantly influence the overall rate of the insertion/β-OR-elimination pathway.

A more informative set of experiments concerns the insertion/β-OEt-elimination of 1,2-dideuterioethyl vinyl ethers illustrated in Scheme 4. *cis*- and *trans*-1,2-dideuterioethylene[32] are readily distinguished by bending vibrations (*cis*-CHD=CHD, 842 cm^{-1}; *trans*-, 988, 726 cm^{-1}) in their IR spectra.[33] When ($^tBu_3SiO)_3TaH_2$ (**1**) reacted with each labeled ethylvinyl ether, complete inversion of ethylene stereochemistry occurred: **1** + *cis*-CHD=CDOEt-d_2 gave *trans*-CHD=CHD, and **1** + *trans*-CHD=CDOEt-d_2 gave *cis*-CHD=CHD. The stereochemistry of the ethylene products is a natural consequence of the standard four-center transition state that arises when the EtO group of the pendent β-OEt-alkyl binds via the eclipsed geometry. A direct exchange pathway would result in retention of ethylene stereochemistry, as shown in Scheme 3 for *trans*-CHD=CDOR-d_2. On the basis of these findings and the β-methoxystyrene experiment, and the direct observation of ($^tBu_3SiO)_3HTaCH_2CH_2OR$ (**2**-CH_2CH_2OR), the insertion/β-OR-elimination process in Scheme 2 was deemed verified.

3. Solution Geometry of ($^tBu_3SiO)_3HTaCH_2CH_2OR$ (2-CH_2CH_2OR). While the eclipsed geometry of the transition state is required for β-OR-elimination, it is also possible that the β-OR group is bound in the ground-state geometry of ($^tBu_3SiO)_3HTaCH_2CH_2OR$ (**2**-CH_2CH_2OR). Variable-temperature ^{1}H NMR spectroscopic studies on the insertion intermediates **2**-*erythro*-CHDCHDOEt and **2**-*threo*-CHDCHDOEt were performed in order to ascertain the likely solution conformation of the β-OEt-alkyl. The $^3J_{HH}$ coupling constant was measured from 23 to −50 °C, and the Karplus relationship,[34] which relates the coupling between two vicinal protons to their dihedral angle (ϕ), was used to determine the dominant conformation. For **2**-*threo*-CHDCHDOEt, Scheme 4 shows that $\phi = 120°$ when Ta and OEt are eclipsed and $\phi = 60°$ in the staggered conformer. The Karplus relationship predicts slightly smaller coupling when $\phi = 60°$; hence, $^3J_{HH'}$ should decrease upon cooling if the staggered conformer is at a lower energy, and only a minimal change from $^3J_{HH} = 4.9$ to 4.3 Hz was observed.

In **2**-*erythro*-CHDCHDOEt, $\phi = 0°$ in the eclipsed conformer versus $\phi = 180°$ in the one where Ta and OEt are staggered. Since coupling is greater when $\phi = 180°$, $^3J_{HH'}$ should increase upon cooling if the staggered geometry is the lower energy conformer, and $^3J_{HH}$ increased slightly from 11.9 to 12.2 Hz. For both isomers, $^3J_{HH}$ changed in the direction predicted by the Karplus relationship if the population of the staggered conformer increased, and the larger absolute magnitude of $^3J_{HH'}$ for **2**-*threo*-CHDCHDOEt versus **2**-*erythro*-CHDCHDOEt was also consistent with the proposed antiperiplanar geometry. Since $^3J_{HH}$ did not change much with temperature in either case, it is likely that **2**-CH_2CH_2OR exists predominantly in the staggered geometry at 23 °C.

4. Structure of ($^tBu_3SiO)_3HTaCH_2CH_2OR$ (2-$CH_2CH_2O^tBu$). The single-crystal X-ray structure of ($^tBu_3SiO)_3HTaCH_2CH_2O^tBu$ (**2**-$CH_2CH_2O^tBu$) constitutes a relatively rare example of a structurally characterized early transition metal alkyl hydride. An abbreviated list of data collection and refinement parameters is given in Table 2, and pertinent bond distances and angles are also tabulated (Table 3). The molecular view in Figure 1 reveals a severely distorted trigonal bipyramidal geometry with an equatorial β-O^{t}Bu-CH_2CH_2 ligand that exhibits a nearly staggered (i.e., dihedral/Ta(C1)C2O4 = 160.7°) conformation. The hydride was located in an equatorial position with d(Ta−H) = 1.72(4) Å, presumably a reflection of its strong σ-donating capacity. The two axial siloxides (d(Ta−O2) = 1.926(3) Å, d(Ta−O3) = 1.913(2) Å) are longer than the equatorial one (d(Ta−O1) = 1.874(3) Å) as expected,[35] and the alkyl occupies the remaining equatorial position with a normal d(Ta−C1) of 2.176(4) Å. While it is somewhat surprising that both axial positions are occupied by the large siloxide ligands, strong σ-donors (e.g., H, alkyl) typically occupy equatorial sites in trigonal bipyramids,[35] and the more electronegative ligands are often axially disposed.[36]

The axial siloxides have a noticeable cant toward the hydride (∠H−Ta−O2 = 81.3(12)°, ∠H−Ta−O3 = 81.3(12)°, ∠O2−Ta−O3 = 154.63(11)°) and away from the more sterically demanding siloxides (∠O1−Ta−O2 = 102.07(11)°, ∠O1−Ta−O3 = 102.49(11)°). If the core were to be described as a square pyramid, Ta−O1 would be apical (∠H−Ta−O1 = 119.1(12)°, ∠O1−Ta−C1 = 112.76(15)°). In view of the rather open H−Ta−C1 angle of 128.1(12)°, one can imagine a rotation

(32) Keul, H.; Choi, H.-S.; Kuczkowski, R. L. *J. Org. Chem.* **1985**, *50*, 3365−3371.
(33) Arnett, R. L.; Crawford, B. L., Jr. *J. Chem. Phys.* **1950**, *18*, 118−126.
(34) (a) Karplus, M. *J. Chem. Phys.* **1959**, *30*, 11−15. (b) Karplus, M. *J. Am. Chem. Soc.* **1963**, *85*, 2870−2871.
(35) Rossi, A. R.; Hoffmann, R. *Inorg. Chem.* **1975**, *14*, 365−374.
(36) Hoffmann, R.; Howell, J. M.; Muetterties, E. L. *J. Am. Chem. Soc.* **1972**, *94*, 3047−3058.

Scheme 4

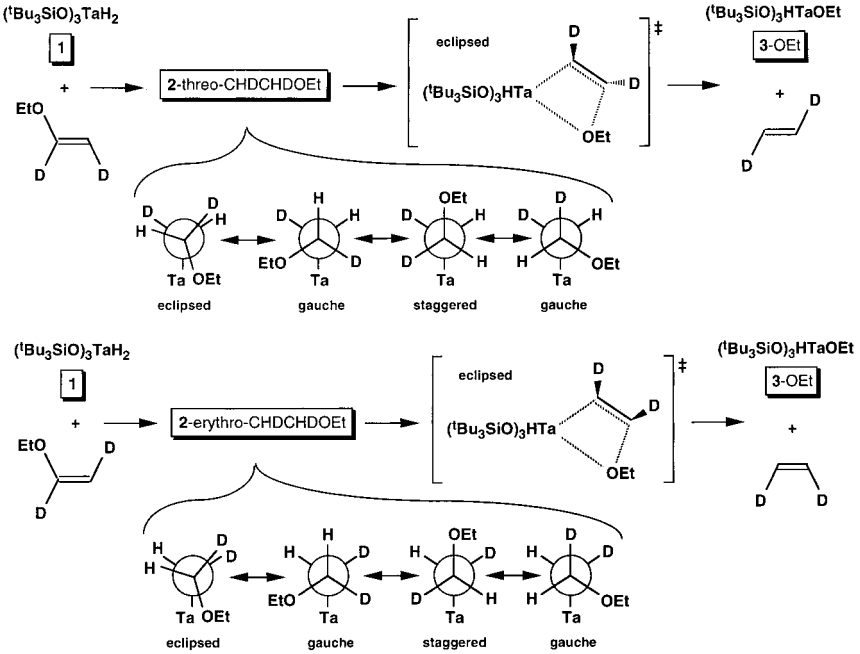

Table 2. Crystallographic Data for Monoclinic (^{t}Bu$_3$SiO)$_3$HTaCH$_2$CH$_2$O^{t}Bu (**2**-CH$_2$CH$_2$O^{t}Bu)

formula	$C_{42}H_{95}O_4Si_3Ta$	T	173(2) K
formula weight	929.40	Z	4
space group	$P2_1/n$	ρ_{calc}	1.214 g/cm^3
λ	0.71073 Å	μ	2.266 mm^{-1}
a	13.2367(10) Å	R [$I > 2\sigma(I)$][a]	0.0396
b	17.7186(13) Å	wR^2 [$I > 2\sigma(I)$][b]	0.0774
c	22.0853(16) Å	GOF[c]	0.986
vol	5083.7(6) Å^3		

[a] $R_1 = \sum||F_o| - |F_c||/\sum|F_o|$. [b] w$R_2 = [\sum w(|F_o| - |F_c|)^2/\sum wF_o^2]^{1/2}$. [c] GOF $= [\sum w(|F_o| - |F_c|)^2/(n - p)]^{1/2}$, n = number of independent reflections (11 575 (R_{int} = 0.0635) of 44 146), p = number of parameters (455).

about the Ta−C1 and C1−C2 bonds that allows the β-OR substituent to coordinate opposite O1 in a six-coordinate transition state for β-OR-elimination. The solid-state structure predicts two inequivalent siloxide ligands in a 2:1 ratio, but only one was observed in the ^{1}H NMR spectrum, consistent with the usual rapid fluxionality accorded d^0 five-coordinate species.

5. Rates of β-OR-Elimination. The direct determination of β-OR-elimination rates was not feasible. The steady-state approximation was invalid since the concentration of (^{t}Bu$_3$SiO)$_3$HTaCH$_2$CH$_2$OR (**2**-CH$_2$CH$_2$OR) was appreciable and varied substantially as the reaction progressed. Additionally, no pre-equilibrium between (^{t}Bu$_3$SiO)$_3$TaH$_2$ (**1**) and vinyl ether substrate was detected (i.e., $k_1 \gg k_{-1}$, $k_2 \gg k_{-1}$) via treatment with the labeled ethyl vinyl ethers. No (^{t}Bu$_3$SiO)$_3$TaH(D) (**1**-*d*), which has a Ta−H resonance in the ^{1}H NMR spectrum upfield from **1**,[31] was observed during the course of this reaction (eq 3). In view of previous estimates of the thermochemistry

$$(^t\mathrm{Bu_3SiO})_3\mathrm{TaH_2}\ (\mathbf{1}) + \mathrm{EtOCD{=}CHD} \xrightarrow{C_7D_8} (^t\mathrm{Bu_3SiO})_3\mathrm{TaH(D)}\ (\mathbf{1}\text{-}d) + \mathrm{EtOCH{=}CHD} \quad (3)$$

of β-H-elimination in (^{t}Bu$_3$SiNH)$_3$ZrCH$_2$CHMe$_2$ ($\Delta H°$(β-H-elim) $\geq$ 16 kcal/mol)[37] and (^{t}Bu$_3$SiO)$_2$(^{t}Bu$_3$SiNH)TiCH$_2$CH$_3$ ($\Delta H°$(β-H-elim) = 16.3 kcal/mol),[38] it is not surprising that the corresponding barrier is substantial in this system. Finally, the β-OR-elimination pathway was further complicated by the reaction of ethylene with the starting dihydride (**1**) to produce (^{t}Bu$_3$SiO)$_3$HTaEt (**4**-Et).[31]

Rate constants for β-OR-elimination (Table 4) were determined by allowing k_1, k_2, and k_3 in Scheme 2 to be parameters in a least-squares fitting of the concentration versus time data of H$_2$C=CHOR, (^{t}Bu$_3$SiO)$_3$TaH$_2$ (**1**), (^{t}Bu$_3$SiO)$_3$HTaCH$_2$CH$_2$OR (**2**-CH$_2$CH$_2$OR), (^{t}Bu$_3$SiO)$_3$HTaOR (**3**-OR), and (^{t}Bu$_3$SiO)$_3$HTaEt (**4**-Et). For each particular vinyl ether present in excess, the hydride resonance of each species was monitored over time by ^{1}H NMR spectroscopy. Figure 2 reveals the observed concentrations versus time data for the H$_2$C=CHO^{n}Pr case plotted in conjunction with simulated data from the calculated rate constants k_1, k_2, and k_3. An excellent agreement between actual and simulated data was obtained for each substrate, indicating the proposed mechanism was at least consistent with the concentrations versus time profile. In principle, such a procedure should have provided k_1 and k_3 in addition to k_2, but experimental difficulties permitted accurate determination of only the latter. As Figure 2 exemplifies, only a fraction of the "rise time" of the intermediate (^{t}Bu$_3$SiO)$_3$HTaCH$_2$CH$_2$OR (**2**-CH$_2$CH$_2$OR) could be determined for R = Me, Et, ^{n}Pr, and Ph. As a consequence, and due to the nature of second-order reactions, a variety of k_1 values (typically (1−5) × 10^{-3} M^{-1} s^{-1}) gave acceptable fits. Inaccuracies in k_3 arise simply from analysis of the small amount of (^{t}Bu$_3$SiO)$_3$HTaEt (**4**-Et) generated at any point in time.

(^{t}Bu$_3$SiO)$_3$TaH$_2$ (**1**) was also treated with divinyl ether, whose two olefinic residues can participate in insertion chemistry. As Scheme 5 illustrates, insertion to give (^{t}Bu$_3$SiO)$_3$HTaCH$_2$CH$_2$OCH=CH$_2$ (**2**-CH$_2$CH$_2$OVy) was observed along with β-OVy-elimination to afford (^{t}Bu$_3$SiO)$_3$HTaOCH=CH$_2$ (**3**-OVy), but the reaction had an additional complication: formation of the double insertion product ((^{t}Bu$_3$SiO)$_3$HTaCH$_2$CH$_2$)$_2$O ((**2**-CH$_2$CH$_2$)$_2$O). In this case, k_1−k_4 were the parameters used to fit

(37) Schaller, C. P.; Cummins, C. C.; Wolczanski, P. T. *J. Am. Chem. Soc.* **1996**, *118*, 591−611.

(38) Bennett, J. L.; Wolczanski, P. T. *J. Am. Chem. Soc.* **1997**, *119*, 10696−10719.

Table 3. Interatomic Distances (Å) and Angles (Deg) Pertaining to ($^tBu_3SiO)_3HTaCH_2CH_2O^tBu$ (**2**-$CH_2CH_2O^tBu$)

Ta−O1	1.874(3)	O1−Si1	1.678(3)	C3−O4	1.430(6)
Ta−O2	1.926(3)	O2−Si2	1.671(3)	C3−C4	1.473(8)
Ta−O3	1.913(2)	O3−Si3	1.671(3)	C3−C5	1.500(11)
Ta−C1	2.176(4)	C1−C2	1.507(6)	C3−C6	1.486(8)
Ta−H	1.72(4)	C2−O4	1.400(5)	C−C_{av}	1.540(8)
SiC−C_{av}	1.537(17)	Si−C_{av}	1.927(7)		
H−Ta−O1	119.1(12)	C1−Ta−O1	112.76(15)	O1−Ta−O2	102.07(11)
H−Ta−O2	81.3(12)	C1−Ta−O2	90.19(14)	O1−Ta−O3	102.49(11)
H−Ta−O3	81.3(12)	C1−Ta−O3	86.16(13)	O2−Ta−O3	154.63(11)
H−Ta−C1	128.1(12)	Ta−C1−C2	117.2(3)	Ta−O1−Si1	178.03(18)
Ta−O2−Si2	156.60(17)	Ta−O3−Si3	163.82(18)	C1−C2−O4	109.1(4)
C2−O4−C3	118.1(4)	O4−C3−C4	108.5(5)	O4−C3−C5	113.2(5)
O4−C3−C6	105.6(5)	C4−C3−C5	104.5(8)	C4−C3−C6	107.1(5)
C5−C3−C6	117.6(7)	O−Si−C_{av}	106.7(12)	C−Si−C_{av}	112.1(9)
Si−C−C_{av}	111.6(12)	C−C−C_{av}	107.2(10)		

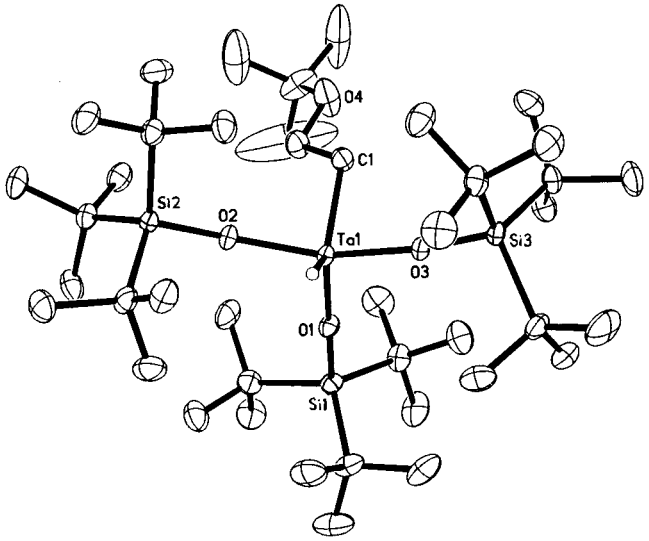

Figure 1. Molecular view of ($^tBu_3SiO)_3HTaCH_2CH_2O^tBu$ (**2**-$CH_2CH_2O^tBu$).

the concentrations vs time profiles of all observables, and β-$OCH_2CH_2TaH(OSi^tBu_3)_3$-elimination from the dinuclear complex (**2**-$CH_2CH_2)_2O$ was not detected.

The data in Table 4 indicate that rates of elimination decreased with increasing size of R, whose Taft E^c_s values[39−42] are also included as objective steric factors for comparison. The inverse rate dependence on the size of R is consistent with a greater difficulty in achieving the eclipsed transition-state geometry for β-OR-elimination from ($^tBu_3SiO)_3HTaCH_2CH_2$-OR (**2**-CH_2CH_2OR). The fastest to eliminate was the vinyl ether **2**-CH_2CH_2OVy, whose sp^2 carbons render this group arguably smaller (note the small value for the "thickness" of the phenyl substituent) than OMe, which is ∼3 times slower.[41] A small declination in rates—about a factor of 3—is then observed for the group OMe > OEt > O^nPr, OPh. It is conceivable that the **2**-CH_2CH_2OVy and **2**-CH_2CH_2OPh manifest electronic contributions to rates of β-OR-elimination, since the vinyl and phenyl substituents are more electron-withdrawing than their alkyl counterparts. However, given the rather minor overall variance in rates, no phenyl substituent studies were undertaken.

There is certainly a major steric influence for the secondary and tertiary substituents, R = ^{i}Pr and ^{t}Bu, neither of which manifests β-OR-elimination at 7 °C within 10 h. β-O^iPr-elimination from ($^tBu_3SiO)_3HTaCH_2CH_2O^iPr$ (**2**-$CH_2CH_2O^iPr$) was observed at elevated temperatures (35−75 °C), enabling $\Delta H^‡ = 22.9(2)$ kcal/mol and $\Delta S^‡ = -7(3)$ eu to be determined from an Eyring plot. The data are consistent with the constrained geometry of the purported four-center transition state for β-O^iPr-elimination and reveal a substantially elevated barrier ($\Delta\Delta G^‡ \approx 4$ kcal/mol) in comparison to the O^nPr case. In summary, steric factors appear to dominate variations in β-OR-elimination rates, as anticipated in view of the four-center transition state in Scheme 4.

Table 4. First-Order Rate Constants for β-OR-Eliminations from ($^tBu_3SiO)_3HTaCH_2CH_2OR$ (**2**-CH_2CH_2OR)[a]

($^tBu_3SiO)_3HTaCH_2CH_2OR$ (**2**-CH_2CH_2OR)	k_2 ($\times 10^4$ s^{-1})	T (±1 °C)	$\Delta G^‡$ (kcal/mol)	E^c_s(R)[b]
2-CH_2CH_2OVy[c]	28(3)	719.6(1)	19.6(1)	
2-CH_2CH_2OMe[d]	9.8(3)	7	20.2(1)	−1.24
2-CH_2CH_2OEt[d]	3.9(3)	7	20.7(1)	−1.62
2-$CH_2CH_2O^nPr$[d]	3.6(1)	7	20.8(1)	−1.91
2-CH_2CH_2OPh[d]	3(1)	7	20.9(2)	−1.01[e]
				−3.82[f]
2-$CH_2CH_2O^iPr$[d,g]	0.095(1)	35		−2.32
	0.31(1)	45		
	1.70(1)	60		
	7.8(2)	75		
2-$CH_2CH_2O^tBu$[h]	<0.002	7		−3.7

[a] Monitored by ^{1}H NMR spectroscopy in C_7D_8. [b] Taft parameters (ref 40) used as a measure of steric bulk of R. [c] Determined from nonlinear, least-squares fitting of the differential forms of the rate expressions to the concentrations vs time data with parameters k_1-k_4 of Scheme 5. [d] Determined from nonlinear, least-squares fitting of the differential forms of the rate expressions to the concentrations vs time data with parameters k_1-k_3 of Scheme 2. [e] "Thickness" of phenyl ring (ref 40). [f] "Width" of phenyl ring (ref 41). [g] Values used in the Eyring plot (35−75 °C). From a weighted nonlinear least-squares fit of the data: $\Delta H^‡ = 22.9(2)$ kcal/mol, $\Delta S^‡ = -7(3)$ eu, $k_2(7\ °C) = 2.0 \times 10^{-7}$ s^{-1}, $\Delta G^‡(7\ °C) = 24.8$ kcal/mol. [h] Estimated assuming <2% of **2**-$CH_2CH_2O^tBu$ β-O^tBu-eliminates in 24 h (7 °C). This is a generous value because no O^tBu-elimination was noted for prolonged periods at 23 °C.

6. Insertion of H_2C=CHO^{i}Pr. Since ($^tBu_3SiO)_3HTaCH_2$-CH_2O^iPr (**2**-$CH_2CH_2O^iPr$) was stable at 7 °C, it was possible to determine the rate of insertion of H_2C=CHO^iPr into a hydride ligand of ($^tBu_3SiO)_3TaH_2$ (**1**). This was a standard second-order reaction, where the disappearance of the dihydride can be expressed as $-d[\mathbf{1}]/dt = k_1[\mathbf{1}][H_2C{=}CHO^iPr]$. Since the initial concentrations of dihydride and isopropyl vinyl ether were known, k_1 was obtained straightforwardly through a plot of $\ln([\mathbf{1}]/[H_2C{=}CHO^iPr])$ vs time. A straight line was obtained whose slope is equivalent to $([\mathbf{1}]_o - [H_2C{=}CHO^iPr]_o)k_1$,[43] yielding a value of $1.9(3) \times 10^{-3}$ M^{-1} s^{-1} for the insertion rate constant, which is included in Table 5.

(39) Taft, R. W., Jr. *J. Am. Chem. Soc.* **1952**, *74*, 3120−3128.
(40) Unger, S. H.; Hansch, C. *Prog. Phys. Org. Chem.* **1976**, *12*, 91−118.
(41) Charton, M. *J. Am. Chem. Soc.* **1969**, *91*, 615−619.
(42) MacPhee, J. A.; Panaye, A.; Dubois, J.-E. *Tetrahedron* **1978**, *34*, 3553−3562.

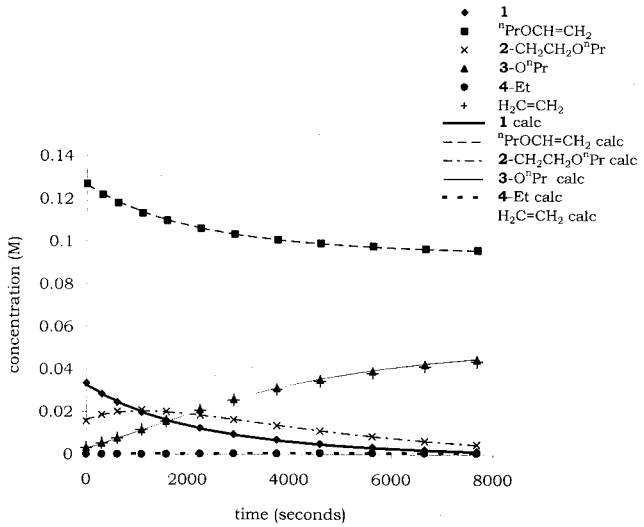

Figure 2. Concentration vs time data for the $H_2C{=}CHO^nPr$ case: experimental points and simulated lines from the fit of k_1, k_2, and k_3 of Scheme 2.

Scheme 5

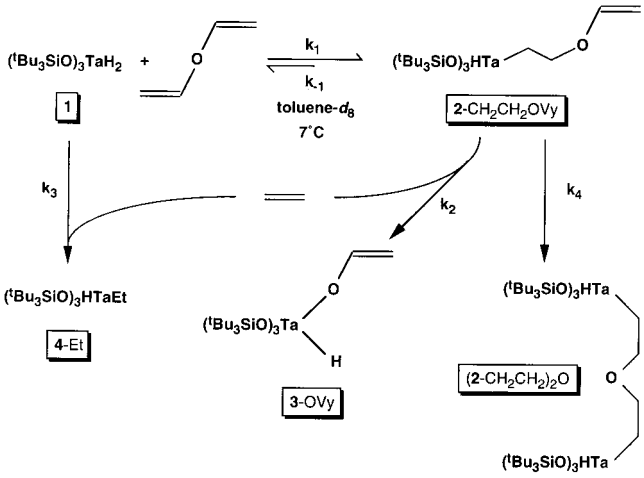

Vinyl Halides. 1. Insertion and *β*-X-Elimination Products. $(^tBu_3SiO)_3TaH_2$ (**1**) was exposed to $H_2C{=}CHX$ (X = F, Cl, Br) at 60 ± 1 °C in toluene-d_8 to afford $(^tBu_3SiO)_3HTaX$ (**3**-X)[31] and $(^tBu_3SiO)_3HTaEt$ (**4**-Et) according to Scheme 6. NMR spectral data for the products are given in Table 1. Complete disappearance of **1** at 60 °C upon treatment with vinyl halides generally took longer than that with the vinyl ethers at 7 °C, and no alkyl-*β*-X-insertion products $(^tBu_3SiO)_3HTaCH_2CH_2X$ (**2**-CH_2CH_2X) were observed in ^1H NMR spectra during the course of the reaction. An approximately even distribution of tantalum-containing products was observed, consistent with a relatively swift insertion of ethylene in comparison to that of $H_2C{=}CHX$.

2. Verification of *β*-X-Elimination. $(^tBu_3SiO)_3TaH_2$ (**1**) did not react with *β*-bromostyrene (eq 4), in concert with the insertion/*β*-X-elimination mechanism in Scheme 6, and incon-

$$(^tBu_3SiO)_3TaH_2 + BrCH{=}CHPh \rightarrow \text{no reaction} \quad (4)$$
1

sistent with a direct exchange pathway related to Scheme 3. As discussed for *β*-methoxystyrene (eq 1), a direct exchange mechanism for production of **3**-X should be relatively insensitive to substitution on the carbon *β* to X. Given the precedent set for the vinyl ether series, no further verification of pathway was considered necessary for the vinyl halide set.

3. Rates of $H_2C{=}CHX$ Insertion. Since $(^tBu_3SiO)_3HTaCH_2CH_2X$ (**2**-CH_2CH_2X) could not be directly observed, a fitting procedure such as that utilized in the vinyl ether cases could not be employed. Two mechanistic scenarios are plausible, given the smooth conversion of $(^tBu_3SiO)_3TaH_2$ (**1**) + $H_2C{=}CHX$ to $(^tBu_3SiO)_3HTaX$ (**3**-X): rate-determining olefin insertion (k_1) or reversible insertion and rate-determining *β*-X-elimination (k_1k_2/k_{-1}). The reversibility of the vinyl halide insertion step was monitored by treating $(^tBu_3SiO)_3TaD_2$ (**1**-d_2) with vinyl chloride (eq 5). No hydrogen (<3%) was incorporated into the

$$2(^tBu_3SiO)_3TaD_2 + H_2C{=}CHCl \xrightarrow[60\ ^\circ C]{C_7D_8} (^tBu_3SiO)_3DTaCl + (^tBu_3SiO)_3DTaEt\text{-}d_2 \quad (5)$$
1-d_2 **3**-D/Cl **4**-D/Et-d_2

starting dideuteride (**1**-d_2)[31] as the reaction progressed, and no hydrogen (<3%) was incorporated into the product $(^tBu_3SiO)_3$-DTaCl (**3**-D/Cl). The ethyl hydride product contained no H in the hydride site, and two deuteriums were distributed over the C_α (~25% D expected) and C_β (~50% D expected) sites of the ethyl group, consistent with insertion of $H_2C{=}CHD$ into the Ta−D bond. Quantitation of the site distribution was precluded by overlapping resonances, but the spectra were roughly consistent with the statistical distribution. Together these analyses indicate that $H_2C{=}CHCl$ insertion is essentially irreversible, thereby eliminating the second mechanistic scenario.

Direct measurements of the $H_2C{=}CHX$ insertion rates were accomplished by monitoring the disappearance of $(^tBu_3SiO)_3$-TaH_2 (**1**) with an excess of vinyl halide. Slightly greater than one-half of the rate of disappearance of **1** was due to reaction with vinyl halide (eqs 6−9);

$$(^tBu_3SiO)_3TaH_2 + H_2C{=}CHX \rightarrow x(^tBu_3SiO)_3HTaX + (1-x)(^tBu_3SiO)_3HTaEt \quad (6)$$
1 **3**-X **4**-Et

$$(-x)\frac{d[\mathbf{1}]}{dt} = k_1[\mathbf{1}][H_2C{=}CHX] \quad (7)$$

$$\frac{d[\mathbf{1}]}{[\mathbf{1}]} = -(k_1/x)[H_2C{=}CHX]\,dt \quad (8)$$

where $z = [\mathbf{3}\text{-X}]/[\mathbf{4}\text{-Et}] = x/(1-x)$ and $x = z/(z+1)$

$$\ln([\mathbf{1}]/[\mathbf{1}]_o) = -k_{obs}t \quad (9)$$

where $k_{obs} = (k_1/x)[H_2C{=}CHX]_o$

the remainder was from its reaction with ethylene. In all cases, $(^tBu_3SiO)_3HTaX$ (**3**-X) and $(^tBu_3SiO)_3HTaEt$ (**4**-Et) grew in at a constant ratio (z = [**3**-X]/[**4**-Et]) throughout the course of reaction, and z was always >1, presumably due to some escape of ethylene to the headspace of the NMR tube. At the end of the runs, a small amount of ethylene can be detected in solution by ^1H NMR spectroscopy. Since only the amount of **3**-X formed reflected the loss of **1** due to vinyl halide insertion, a correction factor that accounts for the stoichiometry must be employed.

(43) Benson, S. W. *The Foundations of Chemical Kinetics*; McGraw-Hill Co.: New York, 1960.

Table 5. Second-Order Rate Constants for $H_2C{=}CHX$ (X = F, Cl, Br, O^iPr) Insertion into $(^tBu_3SiO)_3TaH_2$ (**1**)[a,b]

$H_2C{=}CHX$	[**1**] (M)	[$H_2C{=}CHX$] (equiv)	k_1 [c] ($\times 10^4$ M^{-1} s^{-1})	k_1(av)[c] ($\times 10^4$ M^{-1} s^{-1})	x[d]	$\sigma^+_{\rho,X}$ [e]
$H_2C{=}CHF$	0.0452	6	29.1(7)	24(5)	0.75	−0.07[f]
	0.0452	6	18.0(3)		0.75	
	0.0346	6	23.9(4)		0.70	
	0.0561	9	31.0(3)	27(5)	0.70	
	0.0452	9	19.1(2)		0.75	
	0.0482	9	29.7(5)		0.75	
	0.0560	16	35(1)	27(6)	0.75	
	0.0161	16	26.9(2)		0.80	
	0.0178	16	20.7(2)		0.75	
$H_2C{=}CHCl$	0.0482	6	1.58(1)	1.4(2)	0.55	0.11[f]
	0.0482	6	1.08(1)		0.55	
	0.0533	6	1.53(1)		0.60	
$H_2C{=}CHBr$	0.0469	6	4.89(2)	5.9(8)	0.60	0.15[f]
	0.0452	6	6.74(2)		0.65	
	0.0444	6	6.13(8)		0.65	
	0.0561	10	6.13(2)	6.0(3)	0.65	
	0.0561	10	6.20(3)		0.65	
	0.0573	10	5.6(1)		0.60[g]	
	0.0482	19	2.57(4)	3.3(8)[h]	0.65	
	0.0452	19	4.39(3)		0.70	
	0.0482	19	2.86(3)		0.70	
$H_2C{=}CHO^iPr$[i]	0.0346[i]	0.0720[i]	20.2(4)[i]	19(3)[i]		−0.78[j]
	0.0346[i]	0.0882[i]	16(2)[i]			
	0.0346[i]	0.0869[i]	20.9(1)[i]			
$H_2C{=}CCO_2{}^tBu$			no reaction			0.48[k]

[a] Monitored by ^1H NMR spectroscopy in C_7D_8 at 60 °C unless otherwise noted. [b] r^2 values of ≥0.998 were obtained for all runs unless otherwise noted. [c] Determined from pseudo-first-order plots as described in eqs 6−9 unless otherwise noted. [d] Defined in eq 6. [e] Hammett σ^+_ρ parameters (refs 45, 46) taken to indicate the influence of an electron-withdrawing ($\sigma^+_\rho > 1$) or electron-donating ($\sigma^+_\rho < 1$) substituent on an electron-poor transition state. [f] Hammett σ_I inductive parameters: F, 0.50; Cl, 0.47; Br, 0.45. [g] $r^2 = 0.997$. [h] Aberration from 6 and 10 equiv values perhaps a consequence of $H_2C{=}CHBr$ insolubility (see text). [i] Determined at 7 °C via a second-order plot as described in the text; [$H_2C{=}CHO^iPr$] is expressed in moles per liter. [j] Assumed the same as for OMe. [k] Assumed the same as CO_2Et.

Scheme 6

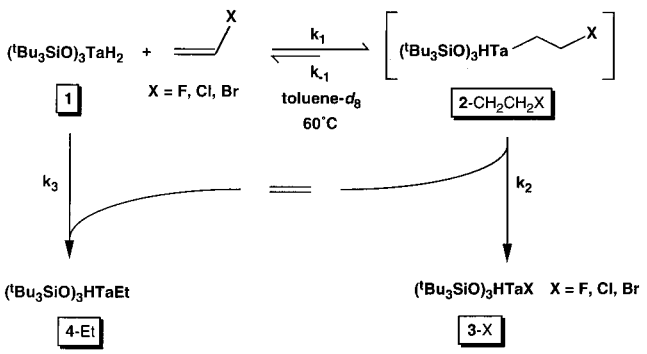

Since $z = x/(1 - x)$, then $x = z/(z + 1)$, and the correction factor $1/x$ can be easily obtained from the product ratio (eqs 7 and 8). The integrated rate expression for the disappearance of **1** (eq 9), where $k_{obs} = (k_1/x)[H_2C{=}CHX]_o$, was valid when the reaction was run under pseudo-first-order conditions in vinyl halide.[43] Values of k_{obs} were obtained from straight-line plots of $-\ln([\mathbf{1}]/[\mathbf{1}]_o)$ vs time for all runs, consistent with the mechanism in Scheme 6 and the kinetics analysis in eqs 7−9, and Table 5 lists the second-order rate constants ascertained from the plots.

Experimental limitations restricted the amount of vinyl halides utilized in the kinetics experiments, and despite the borderline pseudo-first-order conditions in 6 equiv runs, the experiments were generally well behaved. For the case of $H_2C{=}CHF$ at 60 °C, 6, 9, and 16 equiv were used, good agreement was obtained, and the rate constants for insertion were approximately 2.5×10^{-3} M^{-1} s^{-1}. Only 6 equiv runs could be obtained for $H_2C{=}CHCl$ because the solubility of vinyl chloride in toluene proved to be limited. The value of $1.4(2) \times 10^{-4}$ M^{-1} s^{-1} was significantly slower than that for the fluorine derivative and slower than the insertion of $H_2C{=}CHBr$. The vinyl bromide insertion rate constant was $\sim 6 \times 10^{-4}$ M^{-1} s^{-1} according to the 6 and 10 equiv runs, placing it between vinyl fluoride and vinyl chloride. Note that the 19 equiv run was significantly lower than the others, but it is suspected that the number actually reflects the limits of vinyl bromide solubility in toluene and is inaccurate. In summary, there is a modest range (factor of ~18) of insertion rate constants for the vinyl halides, with X = F > Br > Cl.

Alternative Substrates. A selection of other substrates, including vinyl acrylates and ketones, were also submitted with $(^tBu_3SiO)_3TaH_2$ (**1**) in the hopes of obtaining data relevant to the insertion processes of Ziegler−Natta polymerizations. With these substrates, both reduction of the carbonyl moiety and insertion into a Ta−H bond could occur, and a survey conducted in sealed NMR tubes revealed that the former dominated, as expected.

As eq 10 shows, treatment of **1** with ethyl vinyl ketone at 23 °C afforded the 3-pentenoxy hydride $(^tBu_3SiO)_3HTa(OCH(Et)CH{=}CH_2)$ (**3**-OCH(Et)CH=CH_2). Interestingly, at elevated

$$(^tBu_3SiO)_3TaH_2\ (\mathbf{1}) + H_2C{=}CHCOEt \xrightarrow[70\ ^\circ C]{C_7D_8} (^tBu_3SiO)_3HTa(OCH(Et)CH{=}CH_2)\ (\mathbf{3}\text{-OCH(Et)CH}{=}CH_2) \quad (10)$$

temperatures (70 °C), **3**-OCH(Et)CH=CH_2 underwent rearrangement to an apparent oxytantallacyclopentane, $(^tBu_3SiO)_3$-TaOCHEtCH$_2$CH$_2$ (**5**-Et), via insertion of the olefinic residue into the remaining hydride (eq 11). While the aggregation state of **5**-Et is not known for certain, only one isomer was noted, and its solubility suggested a monomeric formulation.

$$\underset{\mathrm{R = H,\ Et}}{\mathbf{3}\text{-OCH(R)CH=CH}_2} \xrightarrow[70\ ^\circ\mathrm{C}]{\mathrm{C_7D_8}} \underset{\mathrm{R = H,\ \mathbf{5}\text{-H};\ Et,\ \mathbf{5}\text{-Et}}}{(^t\mathrm{Bu_3SiO})_3\mathrm{TaOCHRCH_2CH_2}} \quad (11)$$

When $(^t\mathrm{Bu_3SiO})_3\mathrm{TaH_2}$ (**1**) reacted with methyl acrylate, the methoxy hydride $(^t\mathrm{Bu_3SiO})_3\mathrm{HTaOMe}$ (**3**-OMe) and allyloxy hydride $(^t\mathrm{Bu_3SiO})_3\mathrm{HTaOCH_2CH{=}CH_2}$ (**3**-$\mathrm{OCH_2CH{=}CH_2}$) were formed in a 1:1 ratio that was constant with time. Scheme 7 illustrates a mechanism based on initial insertion of the ester carbonyl followed by β-OMe-elimination to afford acrolein, which is rapidly scavenged by **1** to produce **3**-$\mathrm{OCH_2CH{=}CH_2}$. When heated to 70 °C, **3**-$\mathrm{OCH_2CH{=}CH_2}$ also cyclometalated according to eq 11. When *tert*-butyl acrylate was treated with **1**, no reaction took place, indicating that steric protection of

$$\underset{\mathbf{1}}{(^t\mathrm{Bu_3SiO})_3\mathrm{TaH_2}} + \mathrm{H_2C{=}CHCO_2{}^tBu} \xrightarrow[23\ ^\circ\mathrm{C}]{\mathrm{C_7D_8}} \text{no reaction} \quad (12)$$

the ester functionality can be accomplished. Since insertion of the vinyl group did not occur, steric inhibition might also be claimed, but recall that $\mathrm{H_2C{=}CHO{}^tBu}$ inserted rapidly into **1**, and it is unlikely that $\mathrm{H_2C{=}CHCO_2{}^tBu}$ is significantly larger. The ester group $\mathrm{CO_2R}$ is a powerful electron-withdrawing group, which may disfavor olefin binding or hydride transfer.

In principle, the reduction of carbonyl functionalities by $(^t\mathrm{Bu_3SiO})_3\mathrm{TaH_2}$ (**1**) can be used to synthesize $(^t\mathrm{Bu_3SiO})_3\mathrm{HTaOCHR^1R^2}$ (**3**-OR) derivatives, but in practice the greater electrophilicity of **3**-OR relative to that of **1** often offsets its increased steric hindrance, and dialkoxides are formed. For example, treatment of **1** with 1 equiv of acetaldehyde resulted in incomplete reaction and a mixture of $(^t\mathrm{Bu_3SiO})_3\mathrm{HTaOEt}$ (**3**-OEt) and $(^t\mathrm{Bu_3SiO})_3\mathrm{Ta(OEt)_2}$ (**6**-$(\mathrm{OEt})_2$) (eq 13, $n \approx 0.6$). A

$$\underset{\mathbf{1}}{(n+1)/2(^t\mathrm{Bu_3SiO})_3\mathrm{TaH_2}} + \underset{\mathrm{R^1 = H,\ R^2 = Me,\ Et;\ R^1 = R^2 = Me}}{\mathrm{R^1R^2CO}} \xrightarrow[23\ ^\circ\mathrm{C}]{\mathrm{C_7D_8}} n(^t\mathrm{Bu_3SiO})_3\mathrm{HTaOCHR^1R^2} + \underset{\mathbf{6}\text{-}(\mathrm{OEt})_2,\ \mathbf{6}\text{-}(\mathrm{O^nPr})_2,\ \mathbf{6}\text{-}(\mathrm{O^iPr})_2}{\mathbf{3}\text{-OEt},\ \mathbf{3}\text{-O}^n\mathrm{Pr},\ \mathbf{3}\text{-O}^i\mathrm{Pr}} (1-n)/2(^t\mathrm{Bu_3SiO})_3\mathrm{Ta(OCHR^1R^2)_2} \quad (13)$$

similar mixture of $(^t\mathrm{Bu_3SiO})_3\mathrm{HTaO^nPr}$ (**3**-$\mathrm{O^nPr}$) and $(^t\mathrm{Bu_3SiO})_3\mathrm{Ta(O^nPr)_2}$ (**6**-$(\mathrm{O^nPr})_2$) was obtained from propanaldehyde (eq 13, $n \approx 0.6$), but if the ketone or aldehyde is large enough, some stoichiometric control is attained. Multiple insertion was not noticed with ethyl vinyl ketone or methyl acrylate, and with acetone **1** can be converted principally to $(^t\mathrm{Bu_3SiO})_3\mathrm{Ta(O^iPr)_2}$ (**6**-$(\mathrm{O^iPr})_2$) on a preparative scale (eq 13, $n < 0.01$).

Conclusions

Rates of Olefin Insertion. From the observations and direct measurements delineated above, the rates of $\mathrm{H_2C{=}CHX}$ insertion into the hydride bond of $(^t\mathrm{Bu_3SiO})_3\mathrm{TaH_2}$ (**1**) follow the trend X = H ≈ Me ≈ OR ≫ halide. It is difficult to ascertain whether ethylene inserts faster than the vinyl ethers, given the excess of $\mathrm{H_2C{=}CHOR}$ utilized in those experiments, the very minor amounts of $(^t\mathrm{Bu_3SiO})_3\mathrm{HTaEt}$ (**4**-Et) formed, and the corresponding inability to obtain a reliable value for k_3 ($(1-5) \times 10^{-3}\ \mathrm{M^{-1}\ s^{-1}}$) in Scheme 2. From the range of k_1 values generated from the kinetics fits ($k_1 \approx (1-5) \times 10^{-3}\ \mathrm{M^{-1}\ s^{-1}}$), it would appear that the faster vinyl ethers are competitive with ethylene, which is usually taken to be swifter than propylene. The direct measurement of the insertion of $\mathrm{H_2C{=}CHO^iPr}$ of

Scheme 7

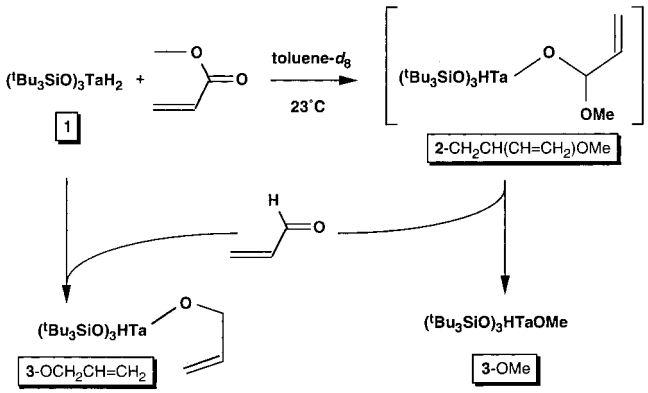

$1.9(3) \times 10^{-3}\ \mathrm{M^{-1}\ s^{-1}}$ (7 °C) appears to support this contention, and comparisons of the individual $\mathrm{H_2C{=}CHOR}$ runs suggest that steric effects are less influential on insertion than on β-OR-elimination; i.e., the "rise times" of the intermediates $(^t\mathrm{Bu_3SiO})_3\mathrm{HTaCH_2CH_2OR}$ (**2**-$\mathrm{CH_2CH_2OR}$) are relatively similar.

In comparing the vinyl ethers and vinyl halides, the latter are decidedly slower, rendering the overall insertion event rate-determining. If the $\mathrm{H_2C{=}CHO^iPr}$ insertion rate at 7 °C is estimated to be $\sim 6 \times 10^{-2}\ \mathrm{M^{-1}\ s^{-1}}$ at 60 °C,[44] its insertion—probably one of the slowest of the vinyl ethers given the bulk of the isopropyl group—is predicted to be at least a factor of 20 faster than that of vinyl fluoride and ~400 times faster than that of vinyl chloride. From the standpoint of Hammett $\sigma^+_{\rho,\mathrm{X}}$ values (Table 5),[45,46] which are arguably a relevant measure of subtituent electron-donating or -withdrawing capacity for the sp^2-vinyl substrates, the strongly electron-donating OR substituents encourage insertion to a greater degree than the halides, which possess intermediate values, and it becomes clearer that the inability of $\mathrm{H_2C{=}CHCO_2{}^tBu}$ to insert may have a significant electronic component, as reasoned above.

Among the halides, the X = F > Br > Cl trend is consistent with a decrease in rate of insertion as the substituent is more electron-withdrawing and less able to π-donate electron density, except it is somewhat unusual to find Br faster than Cl. If it can be assumed that these halides operate more in an inductive capacity (cf. $\sigma_\mathrm{I}(\mathrm{F}) = 0.50$) in this instance, Cl is known to be slightly more inductively withdrawing ($\sigma_\mathrm{I} = 0.47$) than Br ($\sigma_\mathrm{I} = 0.45$), and a rationale is in place.[45,46] To a greater degree than the other halides, a fluoride substituent prefers to be attached to an sp^3 carbon rather than to a more electronegative sp^2 carbon;[47] hence, this factor may also contribute to the overall insertion event.

Referring to path A of Scheme 1, it may be appropriate to view insertion of $\mathrm{H_2C{=}CHX}$ into the tantalum hydride as occurring in two steps: olefin binding and the actual insertion event. Bercaw's seminal studies on olefin insertion of $\mathrm{Cp_2/Cp^*_2\text{-}MH(H_2C{=}CHR)}$ (M = Nb, Ta; R = alkyl, $\mathrm{C_6H_4}$-*p*-Y) clearly show that in the transition state, a slight positive charge develops on C_β, the carbon to which the hydride is migrating.[48] Stabilization of a similar developing positive charge on C_β in the related

(44) The rate was estimated by assuming a $\Delta S^\ddagger$ of −30 eu for the insertion, calculating $\Delta H^\ddagger = 11.5$ kcal/mol at 7 °C from the $\Delta G^\ddagger$ of 19.9 kcal/mol, and recalculating $\Delta G^\ddagger$ at 60 °C to be 21.4 kcal/mol.

(45) Johnson, C. D. *The Hammett Equation*; Cambridge University Press: Cambridge, England, 1973.

(46) Ritchie, C. D.; Sager, W. F. *Prog. Phys. Org. Chem.* **1964**, *2*, 323.

(47) Hine, J.; Mahone, L. G.; Liotta, C. L. *J. Am. Chem. Soc.* **1967**, *89*, 5911−5920.

(48) (a) Doherty, N, M.; Bercaw, J. E. *J. Am. Chem. Soc.* **1985**, *107*, 2670−2682. (b) Burger, B. J.; Santarsiero, B. D.; Trimmer, M. S.; Bercaw, J. E. *J. Am. Chem. Soc.* **1988**, *110*, 3134−3146.

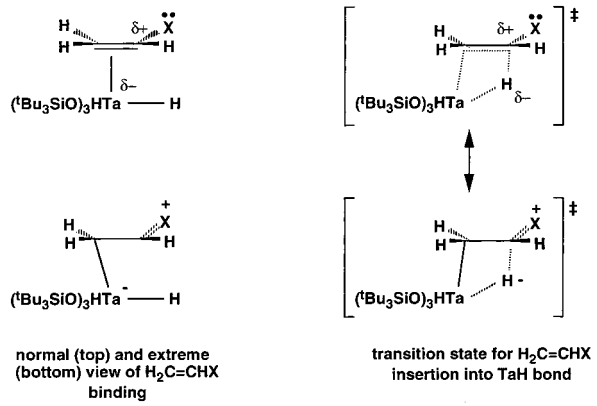

Figure 3. Views of H_2C=CHX binding and the transition state for insertion.

transition state for H_2C=CHX insertion into ($^tBu_3SiO)_3TaH_2$ (**1**) may be operative, as illustrated in Figure 3.

Alternatively, olefin binding may be the critical step, and an extreme zwitterionic view of olefin binding, in which a formal negative charge is placed on tantalum and a positive charge is given to the X substituent, is also shown in Figure 3. The frontier orbital energies of H_2C=CHX lend credence to olefin binding,[49] because electron-donating groups raise the HOMO of the olefin for a better energy match with the d^0 tantalum center, and the coefficient on the α-carbon increases to further desymmetrize the olefin in preparation for the insertion event. The situation herein differs significantly from the Bercaw study in that a d^0 metal center is involved, and its accompanying electrophilicity can greatly polarize the bound olefin and heighten the importance of olefin binding energetics. Electron-donating groups also raise the LUMO, rendering hydride transfer less favorable, but this is counteracted by an increase of the coefficient on the *β*-carbon, which would facilitate H^- transfer; hence, frontier orbital arguments are more ambiguous in predicting the energetics of the insertion transition state. These same rationalizations have been applied to hydroboration, where electron-donating substituents facilitate nucleophilic attack of an alkene on a borane in insertion events that have clear parallels with those of early transition metal hydrides.[50]

In summary, the trend toward swifter insertions for olefins with electron-donating substituents may reflect enhanced binding, i.e., stabilization of an intermediate ($^tBu_3SiO)_3H_2Ta(\eta$-H_2C=CHX), or swifter insertion, i.e., stabilization of the transition state for hydride migration to the olefin. A slight preference for the former rationale may be inferred from frontier orbital arguments. A concerted, one-step mechanism without a formal intermediate binding event could be satisfied through a combination of the above rationales.

Rates of *β*-X-Elimination. As previously discussed, the rates of *β*-OR-elimination shown in Table 4 are simply rationalized on the basis of sterics, and the change in rate-determining step prevents their direct comparison with *β*-X-eliminations. Qualitatively, the halide eliminations are fast relative to insertion, since the putative intermediates, ($^tBu_3SiO)_3HTaCH_2CH_2X$ (**2**-CH_2CH_2X; X = F, Cl, Br), were not detected. For a rough quantitative comparison, assume that the rate of *β*-F-elimination is most closely approximated by *β*-OMe-elimination from ($^tBu_3SiO)_3HTaCH_2CH_2OMe$ (**2**-CH_2CH_2OMe), which was estimated at 60 °C to be ~0.2 s^{-1} by assuming a $\Delta S^‡$ of −7 eu,

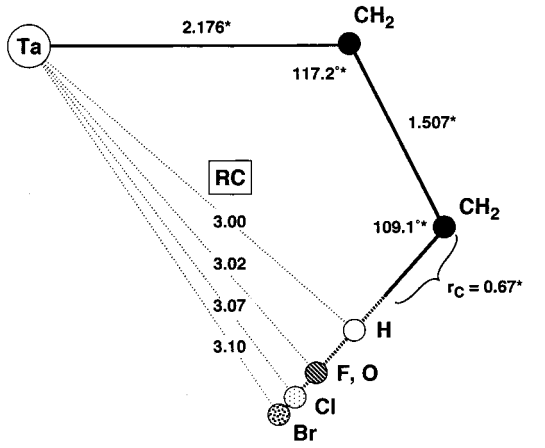

X	r_X(cov) (Å)	$r_X + r_{Ta}$ ~ d(TaX) (Å)	RC - d(TaX) (Å)
H	0.32	1.66	1.34
F	0.72	2.06	0.96
O	0.73	2.07	0.95
Cl	0.99	2.33	0.74
Br	1.14	2.48	0.62

r_{Ta} = 1.34 Å, RC = reaction coordinate (Å)

Figure 4. Probable reaction coordinates (RC) for *β*-X-elimination (X = H, −OR, or F, Cl, and Br) from ($^tBu_3SiO)_3HTaCH_2CH_2X$ (**2**-CH_2CH_2X); asterisks indicate values used from X-ray structural study of ($^tBu_3SiO)_3HTaCH_2CH_2O^tBu$ (**2**-$CH_2CH_2O^tBu$).

the value measured for *β*-O^{i}Pr-elimination from ($^tBu_3SiO)_3HTaCH_2CH_2O^iPr$ (**2**-$CH_2CH_2O^iPr$).[51] As such, *β*-F-elimination is predicted to be ~100 times faster than insertion under standard state conditions, consistent with the absence of **2**-CH_2CH_2F as an observable. From the available data, while *β*-X-eliminations (X = halide) may be safely taken as ≥100 times their respective H_2C=CHX insertions, no actual comparison with *β*-OR-eliminations can be made. At 60 °C, **2**-$CH_2CH_2O^iPr$ eliminates ethylene at a rate similar to the halide cases, but the steric factor of the isopropyl group renders this comparison an oddity.

It is conceivable that *β*-X-elimination may be significantly faster than *β*-OR-elimination, because of the lack of significant steric factors and as a consequence of geometric factors. Figure 4 illustrates simplified reaction coordinates for transfer of a *β*-H, −OR or F, Cl, and Br that were generated using geometric parameters gleaned from the X-ray structural determination of ($^tBu_3SiO)_3HTaCH_2CH_2O^tBu$ (**2**-$CH_2CH_2O^tBu$). The reaction coordinate, here shown as a direct line from the *β*-substituent to the tantalum, is only marginally dependent on the nature of the atom to be transferred. As a consequence, the distance the *β*-group must traverse to become bonded to the tantalum is substantially less as the covalent radii increase;[52] hence, it is likely that Cl and Br may be much swifter in *β*-X-elimination than F, which is comparable to OMe when the steric effects of the methyl are ignored. The reaction coordinate is effectively compressed for the larger atoms in the region of interest.

The thermodynamics of *β*-X-elimination (path D in Scheme 1) can be estimated provided critical bond strengths are known. The reaction involves the breaking of primary metal−carbon and secondary carbon−X bonds, and the formation of metal−X and a carbon−carbon *π*-bond (~65 kcal/mol), thus $\Delta H°_{rxn} = \{D(L_nM-CH_2R) + D(RHPC-X)\} - \{D(L_nM-X) + D(\pi$-

(49) Houk, K. N. *J. Am. Chem. Soc.* **1973**, *95*, 4092−4094.

(50) Smith, K.; Pelter, A. In *Comprehensive Organic Chemistry*, Vol. 8.; Trost, B. M., Fleming, I., Eds.; Pergamon Press: New York, 1991; pp 703−729.

(51) The rate was estimated by assuming a $\Delta S^‡$ of −7 eu for *β*-OMe-elimination, calculating $\Delta H^‡ = 18.3$ kcal/mol at 7 °C from the $\Delta G^‡$ of 20.2 kcal/mol, and recalculating $\Delta G^‡$ at 60 °C to be 20.6 kcal/mol.

(52) Pauling, L. *The Nature of the Chemical Bond*, 3rd ed.; Cornell University Press: Ithaca, New York, 1960.

(CC))}. It is tempting to conclude that greater exothermicity would be accorded X = F > Cl > Br on the basis of stronger D(M−X), but the differences in metal−halide bond strengths are quite substantial (based on CH_3X: D(C−F) ≈ 110, D(C−Cl) ≈ 84, D(C−Br) ≈ 70 kcal/mol)[53] and may compensate. The β-OR cases may manifest greater exothermicity because the D(C−O) of ∼85 kcal/mol may be small compared to that of an early metal−alkoxide bond. Aside from having confidence in the exothermicity of β-X-elimination where X = halide or OR, and the endothermicity of β-H/R-elimination,[37,38] better calculational and experimental input is needed to increase our understanding of the thermochemistry.

Relevance to Ziegler−Natta Polymerization of Polar Comonomers. 1. General. Before any comment is given on the relevance of this model system to true Ziegler−Natta polymerizations, a cautionary statement about the assumptions inherent to such comparisons is necessary. The discussion below will assume that all of the events scrutinized in the model—insertions and β-X/OR-eliminations—scale to the active catalysts. This cannot be rigorously correct because all events in Ziegler−Natta systems are occurring at rates much higher than those observed herein, and as barriers for individual steps become smaller and smaller, rate differences will naturally decline as well. A second caveat concerns the model system itself. Features such as its charge neutrality, the nature of group 5 compounds in comparison to those of group 4 that usually constitute the class of Ziegler−Natta early metal catalysts, and the lack of observed olefin insertions into metal−carbon bonds may render the relevance of the model questionable. In defense of this system, past chemistry clearly supports its characterization as an electrophilic metal center,[54] and one that exhibits reactivity commensurate with many group 4 species, both charged and neutral.

2. Vinyl Halides. The data and observations above do not bode well for the copolymerization of ethylene and vinyl halides. In a growing polyethylene chain (assuming the simple mechanisms of Scheme 1), the rate of propagation is $R_P^e = k_e[L_nMP^+][CH_2CH_2]$, and the rate of chain transfer is $R_{CT}^e = k_{\beta H}[L_nMP^+]$, providing a rough measure of average chain length as $R_P^e/R_{CT}^e \approx (k_e/k_{\beta H})[CH_2CH_2]$. In a corresponding chain of poly(vinyl halide), the average chain length is approximately $R_P^X/R_{CT}^X \approx (k_X/k_{\beta X})[CH_2CHX]$. For the halides, since $k_X'/k_{\beta X} \leq 0.01$ M^{-1}, a maximum concentration of vinyl halide would be needed to offset the intrinsic rate problem presented by the large rate discrepancy favoring β-X-elimination. Assuming the reactions could be carried out in neat vinyl halides, the ∼14 M (X = Br) to ∼18 M (X = F) concentrations would not be enough to offset the more rapid β-X-elimination rate. The problem is compounded by an additional major factor. The rates (k_X') examined herein refer to olefins inserting into *hydrides*, *whereas the true k_X must describe a more energetically difficult insertion into a metal−carbon bond*. Brookhart's studies of ethylene insertion into $[Cp^*\{(MeO)_3P\}MR]^+$ (M = Co, Rh; R = H, polyethylene chain) revealed a 6−10 kcal/mol greater barrier for ethylene insertion into an alkyl, depending on the metal,[55] which roughly translates into a $\sim 10^4-10^7$ rate ratio at 60 °C. As a consequence, the true $k_X/k_{\beta X}$ rate discrepancy is $\leq 10^{-6}-10^{-9}$ M^{-1}, if the values ascribed to the late transition metals translate to early metal systems.

The speed of β-X-elimination relative to that of H_2C═CHX insertion appears to rule out formation vinyl halide homopolymers and copolymers with substantial vinyl halide incorporation, but does it also eliminate the possibility of some minimal incorporation? To circumvent the β-X-elimination problem, it is necessary to expediently move the substituent from the β-position, which occurs when ethylene rapidly inserts following a vinyl halide insertion. If 2×10^{-3} M^{-1} s^{-1} is used for the ethylene insertion rate constant, it is only ∼30 (F)−450 (Cl) times faster than the insertion of the halides, rendering incorporation of vinyl halide infeasible unless the polymerizations are conducted at very high pressures. Polymerizations at low temperature will also tend to enhance the competitiveness of the more entropically disfavored second-order insertion processes relative to the first-order β-X-eliminations.

3. Vinyl Ethers. Vinyl ethers possess a distinct advantage over the vinyl halides in that steric factors can be used to shut down the β-OR-elimination process. Since the rates of insertion of ethylene and H_2C═CHOR (R = small) are relatively similar according to the minimal information gleaned from the fits to Scheme 2, steric control of β-OR-elimination should provide the means of generating copolymers where R = ^{t}Bu or larger. Even the case of R = ^{i}Pr can be tuned, since $k_{OR}'/k_{\beta OR} \approx 10^4$ M^{-1} at 7 °C. Assuming the insertion into a metal−carbon bond is $\sim 10^4-10^7$ slower,[55] the true ratio of insertion to β-OR-elimination is $k_{OR}/k_{\beta OR} \approx 1-10^{-3}$ M^{-1}, and under the most optimistic circumstances with high pressures of ethylene, isopropyl vinyl ether should be incorporated. For smaller R, the small discrepancy between insertion and β-OR-elimination renders alkyl vinyl ether incorporation approaching that of vinyl fluoride difficult.

Unfortunately, an added difficulty arises when vinyl ethers are considered as comonomers. With sufficiently electrophilic metal centers looms the prospect of competing cationic polymerization mechanisms that may obviate any Ziegler−Natta pathways.[56] Such polymerization mechanisms have been observed with cationic group 4 catalysts, and designing catalysts and curtailing impurities to minimize interference from cationic pathways is difficult.

4. Summary. It is unlikely that vinyl halides may be incorporated into polyethylene, even under conditions of maximum [H_2C═CHX] (X = halide) and high pressures of ethylene, which in principle can partially offset the propensity of β-X-elimination from the growing polymer chain. The situation is much better for vinyl ethers, where steric factors can be introduced to inhibit β-OR-elimination and copolymerization can be effected. Cases of H_2C═CHOR where R is small approach those of vinyl halides, and minimal incorporation of the vinyl ether is the best hope, again under conditions of high concentrations of vinyl ether and high pressures of ethylene. Other types of H_2C═CHX are equally difficult to copolymerize when X is an electron-withdrawing functionality, because rates of olefin binding and/or insertion are intrinsically low. When reactive functionalities such as carbonyls are present, steric protection or masking approaches must be used to guard against problematic side reactions.

It is doubtful that any conditions can be found to permit the highly desired copolymerization of ethylene and vinyl halides using standard Ziegler−Natta catalysts. Changes that incorporate a significantly higher barrier for β-X-elimination are necessary for the synthesis of true copolymers, and it is unlikely that such

(53) Data taken from the NIST database, available at http://webbook.NIST.gov.

(54) Wolczanski, P. T. *Polyhedron* **1995**, *14*, 3335−3362 and references therein.

(55) (a) Brookhart, M.; Hauptman, E.; Lincoln, D. M. *J. Am. Chem. Soc.* **1992**, *114*, 10394−10401. (b) Brookhart, M.; Volpe, A. F.; Lincoln, D. M.; Horváth, I. T.; Millar, J. M. *J. Am. Chem. Soc.* **1990**, *112*, 5634−5636.

(56) Baird, M. C. *Chem. Rev.* **2000**, *100*, 1471−1478.

a requirement can be met with conventional catalysts. A different mechanistic approach is mandated by this problem. For example, consider a system where the 2,1-insertion of substituted olefins was greatly favored over 1,2-insertion. A halide or alkoxy functionality in an α-position on a growing polymer chain may be kinetically stabilized relative to a β-X group, thereby permitting further insertions. Popular among current approaches is a switch to later metals where the thermodynamic impetus for β-X-elimination is perhaps mitigated.[19−21] Given the limitations evident in this study, and the necessity of using model complexes to obtain rates slow enough to observe, a calculational investigation of the β-X-elimination problem should prove incisive.

Experimental Section

General Considerations. All manipulations of air-sensitive materials were performed using either glovebox or high-vacuum techniques. Hydrocarbon and ethereal solvents were refluxed over sodium and vacuum-transferred from sodium benzophenone ketyl. Several milliliters of tetraglyme per liter was added to hydrocarbon solvents for solubility purposes. Halogenated solvents were stirred over $CaCl_2$ and then distilled onto $CaCl_2$. Acetone was refluxed over sodium and distilled under Ar onto 4-Å molecular sieves. Acetaldehyde was distilled under Ar. β-Bromostyrene was stirred over sodium and vacuum distilled onto 4-Å molecular sieves. Toluene-d_8 was sequentially dried over sodium and 4-Å molecular sieves. All glassware was either baked in an oven for a minimum of 3 h or flame-dried under dynamic vacuum. $(^tBu_3SiO)_3TaH_2$ (**1**) and $(^tBu_3SiO)_3TaD_2$ (**1**-d_2) were prepared according to the literature procedure.[31] *cis*- and *trans*-1,2-dideuterioethyl vinyl ethers were obtained via the literature procedure[32] from ethyl ethynyl ether in hexanes purchased from Aldrich. Pure ethyl ethynyl ether and ethyl ethynyl ether-*d* were recovered by first generating the lithium salt with LiHNMe. The salt was filtered from hexanes and then quenched with H_2O or D_2O. Isopropyl vinyl ether,[57] divinyl ether,[58] and phenyl vinyl ether[59] were prepared via literature procedures. Methyl vinyl ether and vinyl fluoride were purchased from Lancaster. Vinyl chloride was purchased from Fluka. All other organic reagents were bought from Aldrich.

^1H and $^{13}C\{^1H\}$ NMR spectra were obtained using Varian XL-200, XL-400, INOVA-400, and Unity-500 spectrometers. Chemical shifts were reported relative to toluene-d_7 (^1H, δ 2.09) and toluene-d_8 ($^{13}C\{^1H\}$, δ 20.4). Infrared spectra were recorded on a Nicolet Impact 410 spectrophotometer interfaced to a Gateway PC. Combustion analyses were performed by Robertson Microlit Laboratories in Madison, NJ.

Procedures. 1. $(^tBu_3SiO)_3HTaCH_2CH_2O^tBu$ (2-$CH_2CH_2O^tBu$). A 25-mL round-bottom flask connected to a calibrated gas bulb was charged with $(^tBu_3SiO)_3TaH_2$ (**1**, 200 mg, 0.241 mmol). The apparatus was evacuated, and 5 mL of hexanes was added via vacuum transfer at −78 °C. *tert*-Butyl vinyl ether (0.362 mmol) was condensed into the flask through the gas bulb at −196 °C. The mixture was allowed to warm slowly to 23 °C. The pale yellow solution was stirred for 6 h, and the volatiles were removed in vacuo to yield an off-white powder. X-ray-quality crystals were grown by slow cooling to −35 °C of a concentrated hexanes solution. Anal. Calcd for $C_{42}H_{95}O_4Si_3Ta$: C, 54.27; H, 10.32. Found: 55.67; H, 10.75.

2. $(^tBu_3SiO)_3HTaO^iPr$ (3-O^iPr). A 10-mL round-bottom flask connected to a calibrated gas bulb was charged with $(^tBu_3SiO)_3TaH_2$ (**1**, 100 mg, 0.121 mmol). The apparatus was evacuated, and 5 mL of hexanes was added via vacuum transfer at −78 °C. Acetone (0.182 mmol) was condensed into the flask through the gas bulb at −196 °C. The mixture was allowed to warm slowly to 23 °C. The pale yellow solution was stirred for 12 h, and the volatiles were removed in vacuo to yield an off-white powder. Anal. Calcd for $C_{39}H_{89}O_4Si_3Ta$: C, 52.78; H, 10.13. Found: C, 51.10; H, 9.59.

3. $(^tBu_3SiO)_3HTa^nPr$ (4-^{n}Pr). A 10-mL round-bottom flask connected to a calibrated gas bulb was charged with $(^tBu_3SiO)_3TaH_2$ (**1**, 161 mg, 0.195 mmol). The apparatus was evacuated, and 5 mL of pentanes was added via vacuum transfer at −78 °C. Propylene (0.390 mmol) was added to the flask through the gas bulb at −196 °C. The mixture was allowed to warm slowly to 23 °C. The pale yellow solution was stirred for 12 h, after which the volatiles were removed in vacuo to yield a white powder. Anal. Calcd for $C_{39}H_{89}O_3Si_3Ta$: C, 53.76; H, 10.30. Found: C, 54.00; H, 10.40.

4. $(^tBu_3SiO)_3HTaOEt$ (3-OEt) and $(^tBu_3SiO)_3Ta(OEt)_2$ (6-$(OEt)_2$). A 10-mL round-bottom flask connected to a calibrated gas bulb was charged with $(^tBu_3SiO)_3TaH_2$ (**1**, 100 mg, 0.121 mmol). The apparatus was evacuated, and 5 mL of hexanes was added via vacuum transfer at −78 °C. Acetaldehyde (0.182 mmol) was added to the flask through the gas bulb at −196 °C. The mixture was allowed to warm slowly to 23 °C. The pale yellow solution was stirred for 12 h, and the volatiles were removed in vacuo to yield an off-white powder.

5. $(^tBu_3SiO)_3HTaO^nPr$ (3-O^nPr) and $(^tBu_3SiO)_3Ta(O^nPr)_2$ (6-$(O^nPr)2$). A 10-mL round-bottom flask connected to a calibrated gas bulb was charged with $(^tBu_3SiO)_3TaH_2$ (**1**, 100 mg, 0.121 mmol). The apparatus was evacuated, and 5 mL of hexanes was added via vacuum transfer at −78 °C. Propionaldehyde (0.182 mmol) was added to the flask through the gas bulb at −196 °C. The mixture was allowed to warm slowly to 23 °C. The pale yellow solution was stirred for 12 h, after which the volatiles were removed in vacuo to yield an off-white powder.

NMR Tube Reactions. General. An NMR tube attached to a 14/20 ground glass joint was flame-dried and charged with $(^tBu_3SiO)_3TaH_2$ (**1**, typical ∼35 mg, 0.04 mmol) in a dry box. A flame-dried calibrated gas bulb was attached to the adapter, and the assembly was degassed. Toluene-d_8 was vacuum-transferred into the tube at −196 °C. Reagent was condensed into the tube at −196 °C through the gas bulb. The tube was sealed with a torch under dynamic vacuum.

6. $(^tBu_3SiO)_3HTaOCH(Et)CH$═$CH_2$). An NMR tube was charged with $(^tBu_3SiO)_3TaH_2$ (**1**, 32 mg, 0.03858 mmol) in a dry box. A 90.6-mL gas bulb was attached to the adapter and the assembly degassed. Toluene-d_8 was vacuum-transferred into the tube at −196 °C. Ethyl vinyl ketone (50.7 Torr, 0.250 mmol) was condensed into the tube at −196 °C. The tube was sealed with a torch under dynamic vacuum. The tube was warmed to 23 °C, and the conversion to product was immediate.

7. $(^tBu_3SiO)_3\overline{TaOCH(Et)CH_2CH_2}$ (5-Et). The sealed NMR tube containing a solution of **3**-OC(Et)HCH═CH_2 and residual ethyl vinyl ketone in toluene-d_8 was heated at 70 °C for 12 h to generate **5**-Et.

8. $(^tBu_3SiO)_3HTaOCH_2CH$═CH_2 (3-OCH_2CH═CH_2) and $(^tBu_3SiO)_3HTaOMe$ (3-OMe). An NMR tube was charged with $(^tBu_3SiO)_3TaH_2$ (**1**, 35 mg, 0.0422 mmol) in a dry box. A 90.6-mL gas bulb was attached to the adapter and the assembly degassed. Toluene-d_8 was vacuum-transferred into the tube at −196 °C. Methyl acrylate (44.6 Torr, 0.220 mmol) was condensed into the tube at −196 °C. The tube was sealed with a torch under dynamic vacuum. After the reaction mixture warmed to 23 °C, the product was immediately observed, along with an equimolar amount of **3**-OMe.

9. $(^tBu_3SiO)_3\overline{TaOCH_2CH_2CH_2}$ (5-H). The sealed NMR tube containing a toluene-d_8 solution of **3**-OCH_2CH═CH_2 (along with **3**-OMe and residual divinyl ether) was heated at 70 °C for 12 h to form **5**-H.

General Kinetics Procedures. For the vinyl ethers, a measured amount (typically ∼35 mg, ∼0.04 mmol) of $(^tBu_3SiO)_3TaH_2$ (**1**) was added to a flame-dried 5-mm NMR tube attached to a 14/20 joint. The adapted NMR tube was connected to a calibrated gas bulb, and 1 mL of toluene-d_8 was vacuum-transferred into the evacuated assembly. Substrate was then condensed into the solution via the gas bulb at −196 °C, and the tube was sealed with a torch under active vacuum. For the vinyl halides, a stock solution of **1** in toluene-d_8 was prepared in a 10-mL volumetric flask in a dry box. An aliquot of this solution (typically ∼0.60 mL, 0.03 mmol) was added to an NMR tube attached to a 14/20 ground glass joint and a calibrated gas bulb. The assembly was subjected to three freeze−pump−thaw degas cycles. The vinyl reagent was submitted to the NMR tube through the gas bulb at −196

(57) Watanabe, W. H.; Conlon, L. E. *J. Am. Chem. Soc.* **1957**, *79*, 12828-2833.

(58) Cretcher, L. H.; Koch, J. A.; Pittenger, W. H. *J. Am. Chem. Soc.* **1925**, *47*, 1173−1177.

(59) McClelland, R. A. *Can. J. Chem.* **1977**, *55*, 548−551.

°C. The tube was sealed under dynamic vacuum. The rate at which the concentration of a species changed with time was typically monitored by measuring the area under its hydride resonance. Pre-acquisiton delays of increasing time intervals were utilized to observe the completion of each reaction in the NMR spectrometer probe. Sixteen transients were taken each time a spectrum was acquired. The relaxation times ($T1$) of hydride resonances were determined to be ~1 s by inversion recovery following calibration of a 90° pulse width for the signal. $D1$ was set to $6T1 = 6$ s. The temperature at which the reaction was monitored was regulated by the NMR probe. An exact measurement of the reaction temperature was obtained by running an internal calibration with a tube of ethylene glycol. All runs were taken out to a minimum of four half-lives. β-OR-elimination rates were obtained from nonlinear least-squares fitting to the differential forms of the rate expressions. Least-squares fitting was performed with a modified Powell algorithm to minimize the sum-of-squares deviations between observed data and model calculations. Multiple simulations were performed to the minimize 95% confidence range.[60] Vinyl halide insertion rates were obtained by plotting the integrated rate expression for disappearance of **1** under pseudo-first-order conditions to obtain a straight line; the slope of the resulting line was directly related to the insertion rate constant.

Determination of Ethylene-d_2 Stereochemistry. A sealed NMR tube in which ethylene-d_2 had been evolved was placed in a tube-cracker connected to a 180° needle valve. This apparatus was evacuated. The tube was cracked while the system was closed to active vacuum. After 5 min, the assembly was cooled to −78 °C. After 15 min, the volatiles were condensed into an evacuated round-bottom flask at −196 °C. This flask was warmed to 23 °C, and its contents were allowed to expand into an evacuated IR cell. After 10 min, the IR cell was sealed and removed to the IR spectrophotometer. Absorbance measurements were taken after 16 scans at a resolution of 1 cm^{-1}. *trans*-1,2-Dideuterioethylene has two strong out-of-plane vibrations at 987 and 725 cm^{-1}. *cis*-1,2-Dideuterioethylene has one strong out-of-plane vibration at 842 cm^{-1}.[33]

(60) MicroMath^R SCIENTIST, Experimental Data Fitting; MicroMath, Inc., 1986−1995.

X-ray Structure Determination of (^{t}Bu$_3$SiO)$_3$HTaCH$_2$CH$_2$O^{t}Bu (2-CH$_2$CH$_2$O^{t}Bu). A few milligrams of crystals (vide supra) were suspended in Paratone oil on a glass slide. Under a microscope, a single colorless block (0.20 × 0.10 × 0.040 mm^3) was picked up in a 100-μm rayon fiber loop epoxied to a metal fiber. X-ray diffraction data were collected on a Siemens SMART system ($\lambda = 0.71073$) employing a 1 K CCD detector and an Oxford Cryostream set at 165 K. Observed intensities were corrected for Lorentz and polarization effects, and a semiempirical absorption correction was applied (SADABS). The structure was solved by direct methods (SHELXTL). The hydride was located and refined isotropically, while the remaining hydrogen atoms were calculated and included in the model. The structure was refined by full-matrix least-squares on F^2 using isotropic thermal parameters for all non-hydrogen atoms. The largest difference peak and hole were 0.988 and −1.045 e $Å^{-3}$.

Acknowledgment. We thank Emil B. Lobkovsky for experimental assistance, and Prof. Barry Carpenter for consultation. We gratefully acknowledge contributions from the National Science Foundation (CHE-9816134), The Dow Chemical Co., and Cornell University.

Supporting Information Available: Plots of the kinetics fits of Schemes 2 and 5, and a summary of crystal data, encompassing data collection and solution/refinement, atomic coordinates, isotropic and anisotropic temperature factors, hydrogen atom coordinates, bond lengths and bond angles for (^{t}Bu$_3$SiO)$_3$HTaCH$_2$CH$_2$O^{t}Bu (**2**-CH$_2$CH$_2$O^{t}Bu) (PDF). This material is available free of charge via the Internet at http://pubs.acs.org.

JA003315N